

1 **Role of a key microphysical factor in mixed-phase stratocumulus clouds and their**  
2 **interactions with aerosols**

3

4 Seoung Soo Lee<sup>1,2,3</sup>, Chang-Hoon Jung<sup>4</sup>, Jinho Choi<sup>5</sup>, Young Jun Yoon<sup>6</sup>, Junshik Um<sup>5,7</sup>,  
5 Youtong Zheng<sup>8</sup>, Jianping Guo<sup>9</sup>, Manguttathil. G. Manoj<sup>10</sup>, Sang-Keun Song<sup>11</sup>

6

7 <sup>1</sup>Science and Technology Corporation, Hampton, Virginia

8 <sup>2</sup>Earth System Science Interdisciplinary Center, University of Maryland, College Park,  
9 Maryland, USA

10 <sup>3</sup>Research Center for Climate Sciences, Pusan National University, Busan, Republic of  
11 Korea

12 <sup>4</sup>Department of Health Management, Kyungin Women's University, Incheon, Republic of  
13 Korea

14 <sup>5</sup>Department of Atmospheric Sciences, Pusan National University, Busan, Republic of  
15 Korea

16 <sup>6</sup>Korea Polar Research Institute, Incheon, Republic of Korea

17 <sup>7</sup>Institute of Environmental Studies, Pusan National University, Busan, Republic of Korea

18 <sup>8</sup>Department of Earth and Atmospheric Sciences, University of Houston, Houston, Texas,  
19 USA

20 <sup>9</sup>State Key Laboratory of Severe Weather, Chinese Academy of Meteorological Sciences,  
21 Beijing 100081, China

22 <sup>10</sup>Advanced Centre for Atmospheric Radar Research, Cochin University of Science and  
23 Technology, Kerala, India

24 <sup>11</sup>Department of Earth and Marine Sciences, Jeju National University, Jeju, Republic of  
25 Korea

26

27

28

29

30

31

32

33

34

35

36

37

38

39

40

41

42

43

44

45

46 Corresponding author: Seoung Soo Lee, Chang-Hoon Jung and Sang-Keun Song

47 Office: (303) 497-6615

48 Cell: (609) 375-6685

49 Fax: (303) 497-5318

50 E-mail: [cumulss@gmail.com](mailto:cumulss@gmail.com), [slee1247@umd.edu](mailto:slee1247@umd.edu)

51

52

53

54 **Abstract**

55

56 This study examines the ratio of ice crystal number concentration (ICNC) to cloud droplet  
57 number concentration (CDNC), which is ICNC/CDNC, in mixed-phase stratocumulus  
58 clouds. This examination is performed using a large-eddy simulation (LES) framework and  
59 one of efforts toward a more general understanding of mechanisms controlling cloud  
60 development, aerosol-cloud interactions and impacts of ice processes on them in mixed-  
61 phase stratocumulus clouds. For the examination, this study compares a case of polar  
62 mixed-phase stratocumulus clouds to that of midlatitude mixed-phase stratocumulus  
63 clouds with weak precipitation. It is found that ICNC/CDNC plays a critical role in making  
64 differences in cloud development with respect to the relative proportion of liquid and ice  
65 mass between the cases by affecting in-cloud latent-heat processes. Note that this  
66 proportion has an important implication for cloud radiative properties and thus climate. It  
67 is also found that ICNC/CDNC plays a critical role in making differences in interactions  
68 between clouds and aerosols and impacts of ice processes on clouds and their interactions  
69 with aerosols between the cases by affecting in-cloud latent-heat processes. Findings of  
70 this study suggest that ICNC/CDNC can be a simplified general factor that contributes to  
71 a more general understanding and parameterizations of mixed-phase clouds, their  
72 interactions with aerosols and roles of ice processes in them.

73

74

75

76

77

78

79

80

81

82

83

84

## 1. Introduction

85  
86  
87 Stratiform clouds (e.g., stratus and stratocumulus clouds) have significant impacts on  
88 climate (Warren et al. 1986; Stephens and Greenwald 1991; Hartmann et al. 1992; Hahn  
89 and Warren 2007; Wood, 2012; Dione et al., 2019; Zheng et al., 2021). Since  
90 industrialization, aerosol concentrations have increased and this has had impacts on  
91 stratiform clouds and climate (Twomey, 1974; Albrecht, 1989; Ackerman et al., 2004).  
92 However, our level of understanding of these clouds and impacts has been low and this has  
93 caused the highest uncertainty in the prediction of future climate (Ramaswamy et al., 2001;  
94 Forster et al., 2007; Knippertz et al., 2011; Hannak et al., 2017). Stratiform clouds can be  
95 classified into warm and mixed-phase clouds. Mixed-phase stratiform clouds involve ice  
96 processes and frequently form in midlatitude and polar regions. When mixed-phase clouds  
97 are associated with convective clouds, they can form even in the tropical region. Most  
98 previous studies have focused on warm clouds and their interactions with aerosols, whereas  
99 the mixed-phase stratiform clouds and their interactions with aerosols are poorly  
100 understood mainly due to the more complex ice processes. Hence, mixed-phase stratiform  
101 clouds and their interactions with aerosols account for the uncertainty more than warm  
102 clouds and their interactions with aerosols (Ramaswamy et al., 2001; Forster et al., 2007;  
103 Wood, 2012; IPCC, 2021; Li et al., 2022).

104 The relative proportion of liquid mass, which can be represented by liquid-water  
105 content (LWC) or liquid-water path (LWP), and ice mass, which can be represented by ice-  
106 water content (IWC) or ice-water path (IWP), in mixed-phase stratiform clouds plays a  
107 critical role in cloud radiative properties and thus their climate feedbacks (Tsushima et  
108 al., 2006; Choi et al., 2010 and 2014; Gettelman et al., 2012; Zhang et al., 2019). The  
109 relative proportion is defined to be IWC (IWP) over LWC (LWP) or IWC/LWC  
110 (IWP/LWP) in this study. Motivated by this and the above-mentioned uncertainty, this  
111 study aims to improve our understanding of mixed-phase stratiform clouds and their  
112 interactions with aerosols with the emphasis on ice processes and IWC/LWC (or  
113 IWP/LWP).

114 Lee et al. (2021) have investigated mixed-phase stratocumulus clouds in a midlatitude  
115 region and found that microphysical latent-heat processes are more important in the

116 development of mixed-phase stratiform clouds and their interactions with aerosols than  
117 entrainment and sedimentation processes. Lee et al. (2021) have found that a microphysical  
118 factor, the ratio of ice crystal number concentration (ICNC) to cloud droplet number  
119 concentration (CDNC) or ICNC/CDNC, play an important role in latent processes, the  
120 development of mixed-phase stratiform clouds and their interactions with aerosols. In  
121 particular, Lee et al. (2021) have found that IWC/LWC or IWP/LWP is strongly affected  
122 by ICNC/CDNC. This is because water vapor deposits on the surface of ice crystals, while  
123 it condenses on droplets. As a result, ice crystals act as sources of deposition and droplets  
124 act as sources of condensation. Consequently, ice crystals act as sources of IWC (or IWP)  
125 and droplets act as sources of LWC (or LWP). More ice crystals and droplets provide the  
126 greater integrated surface area of ice crystals and droplets and induce more deposition and  
127 condensation, respectively, for a given environmental condition (Lee et al., 2009; Khain et  
128 al., 2012; Fan et al., 2018; Chua and Ming, 2020; Lee et al., 2021). The higher  
129 ICNC/CDNC means more ice crystals or sources of deposition per a droplet as a source of  
130 condensation in a given group of ice crystals and droplets. Thus, the higher ICNC/CDNC  
131 enables more deposition per unit condensation to occur, which can raise IWC/LWC or  
132 IWP/LWP.

133 Mixed-phase stratocumulus clouds in different regions are known to have different  
134 IWC/LWC or IWP/LWP and aerosol-cloud interactions (e.g., Choi et al., 2010 and 2014;  
135 Zhang et al., 2019). Lots of factors such as environmental conditions, which can be  
136 represented by variables such as temperature, humidity and wind shear, and macrophysical  
137 factors one of which is the relative locations of ice-crystal and droplet layers, can explain  
138 those differences. Choi et al. (2010 and 2014) and Zhang et al. (2019) have shown that as  
139 temperature lowers, IWC/LWC or IWP/LWP tends to increase and indicated that  
140 temperature is a primary environmental condition to explain the differences in IWC/LWC  
141 among different regions or clouds. However, Choi et al. (2010 and 2014) and Zhang et al.  
142 (2019) have not discussed process-level mechanisms that govern the role of temperature in  
143 those differences.

144 It is important to establish a general principle that explains the differences in  
145 LWC/LWC and aerosol-cloud interactions among regions, since the general principle is  
146 useful in the development of a more general or comprehensive parameterization of

147 stratocumulus clouds and their interactions with aerosols for climate models. This  
148 contributes to the better prediction of future climate, considering that the absence of the  
149 comprehensive parameterization has been considered one of the biggest obstacles to the  
150 better prediction (Ramaswamy et al., 2001; Foster et al., 2007; Stevens and Feingold, 2009).

151 As a way of contributing to the establishment of the general principle, this study  
152 attempts to take ICNC/CDNC as a general factor, which can constitute the general principle,  
153 to explain the differences in IWC/LWC (or IWP/LWP) and aerosol-cloud interactions  
154 among clouds. This study also attempts to elucidate how ice processes differentiate mixed-  
155 phase stratiform clouds from warm clouds in terms of cloud development and its  
156 interactions with aerosols, and how this differentiation varies among cases of mixed-phase  
157 stratiform clouds with different ICNC/CDNC values. This attempt is valuable, considering  
158 that in general, the establishment of the general principle for stratocumulus clouds and their  
159 interactions with aerosols has been progressed much less than that for other types of clouds  
160 such as convective clouds and their interactions with aerosols. The attempt is valuable, also  
161 considering that our level of understanding of how ice processes differentiate mixed-phase  
162 stratiform clouds and their interactions with aerosols from much-studied warm clouds and  
163 their interactions with aerosols has been low. Here, we want to emphasize that this study  
164 does not aim to gain a fully established general principle, but aims to test the factor that  
165 can be useful to move ahead on our path to a more complete general principle. Hence, this  
166 study should be regarded a steppingstone to the established principle, and should not be  
167 considered a perfect study that get us the fully established principle. Taking into account  
168 the fact that even attempts to provide general factors for the general principle have been  
169 rare, the fulfilment of the aim is likely to provide us with valuable preliminary information  
170 that streamlines the development of a more established general principle.

171 For the attempt, this study investigates a case of mixed-phase stratiform clouds in the  
172 polar region. Via the investigation, this study aims to identify process-level mechanisms  
173 that control the development of those clouds and their interactions with aerosols, and the  
174 impact of ice processes on the development and interactions using a large-eddy simulation  
175 (LES) framework. Then, this study compares the mechanisms in the case of polar clouds  
176 to those in a case of midlatitude clouds which have been examined by Lee et al. (2021).  
177 This comparison is based on Choi et al. (2010 and 2014) and Zhang et al. (2019) which

178 have shown that temperature is an important factor which explains the differences in  
179 IWC/LWC among regions or clouds. Due to significant differences in latitudes, noticeable  
180 differences in the temperature of air are between the polar and midlatitude cases. Hence,  
181 through this comparison, this study looks at the role of temperature in those differences in  
182 IWC/LWC and associated aerosol-cloud interactions. More importantly than that, as a way  
183 of identifying process-level mechanisms that control the role of temperature, this study  
184 tests how ICNC/CDNC as the general factor is linked to the role of temperature, using the  
185 LES framework. Through this test, this study also identifies process-level mechanisms that  
186 control how ICNC/CDNC affects roles of ice processes in the differentiation between  
187 mixed-phase stratiform and warm clouds in terms of cloud development and its interactions  
188 with aerosols, and causes the variation of the differentiation between the cases of mixed-  
189 phase stratiform clouds.

190

## 191 **2. Case, model and simulations**

192

### 193 **2.1 LES model**

194

195 LES simulations are performed by using the Advanced Research Weather Research and  
196 Forecasting (ARW) model. A bin scheme, which is detailed in Khain et al. (2000) and  
197 Khain et al. (2011), is adopted by the ARW for the simulation of microphysics. Size  
198 distribution functions for each class of hydrometeors, which are classified into water drops,  
199 ice crystals (plate, columnar and branch types), snow aggregates, graupel and hail, are  
200 represented with 33 mass doubling bins, i.e., the mass of a particle  $m_k$  in the  $k$ th bin is  
201 determined as  $m_k = 2m_{k-1}$ . Each of hydrometeors has its own terminal velocity that varies  
202 with the hydrometeor mass and the sedimentation of hydrometeors is simulated using their  
203 terminal velocity.

204 Size distribution functions for aerosols, which act as cloud condensation nuclei  
205 (CCN) and ice-nucleating particles (INP), adopt the same mass doubling bins as for  
206 hydrometeors. The evolution of aerosol size distribution and associated aerosol  
207 concentrations at each grid point is controlled by aerosol sinks and sources such as aerosol  
208 advection, turbulent mixing, activation and aerosol regeneration via the evaporation of

209 droplets and the sublimation of ice crystals. Aerosol regeneration follows the method  
210 similar to that as described in Xue et al. (2010). It is assumed that aerosols do not fall down  
211 by themselves and move around by airflow that is composed of horizontal flow, updrafts,  
212 downdrafts and turbulent motions. When aerosols move with airflow, it is assumed that  
213 they move with the same velocity as airflow. Taking activation as an example of the  
214 evolution of aerosol size distribution, the bins of the aerosol spectra that correspond to  
215 activated particles are emptied. Activated aerosol particles are included in hydrometeors  
216 and move to different classes and sizes of hydrometeors through collision-coalescence. In  
217 case hydrometeors with aerosol particles precipitate to the surface, those particles are  
218 removed from the atmosphere.

219 The large energetic turbulent eddies are directly resolved by the LES framework, and  
220 the effects of the smaller subgrid-scale turbulent motions on the resolved flow are  
221 parameterized based on a most widely used method that Smagorinsky (1963) and Lilly  
222 (1967) proposed. In this method, the mixing time scale is defined to be the norm of the  
223 strain rate tensor (Bartosiewicz and Duponcheel, 2018). A cloud-droplet nucleation  
224 parameterization based on Köhler theory represents cloud-droplet nucleation. Arbitrary  
225 aerosol mixing states and aerosol size distributions can be fed to this parameterization. To  
226 represent heterogeneous ice-crystal nucleation, the parameterizations by Lohmann and  
227 Diehl (2006) and Möhler et al. (2006) are used. In these parameterizations, contact,  
228 immersion, condensation-freezing, and deposition nucleation paths are all considered by  
229 taking into account the size distribution of INP, temperature and supersaturation.  
230 Homogeneous aerosol (or haze particle) and droplet freezing is  
231 also considered following the theory developed by Koop et al. (2000).

232 The bin microphysics scheme is coupled to the Rapid Radiation Transfer Model  
233 (RRTM; Mlawer et al., 1997). The effective sizes of hydrometeors, which are calculated  
234 in the bin scheme, are fed into the RRTM as a way of considering effects of the effective  
235 sizes on radiation. The surface process and resultant surface heat fluxes are simulated by  
236 the interactive Noah land surface model (Chen and Dudhia, 2001).

237

## 238 **2.2 Case and simulations**

239



### 2.2.1 Case and standard simulations

240

241

242 In the Svalbard area, Norway, a system of mixed-phase stratocumulus clouds existed over  
243 the horizontal domain marked by a red rectangle in Figure 1 and a period between 02:00  
244 and 10:00 local solar time (LST) on March 29<sup>th</sup>, 2017. These clouds are observed by a  
245 ground station which is a part of the Cloudnet observation network and marked by a dot in  
246 Figure 1. The Cloudnet observation has been established to provide a systematic evaluation  
247 of clouds in forecast and climate models. The Cloudnet observation aims to establish a  
248 number of ground-based remote sensing sites, which would all be equipped with a specific  
249 array of instrumentation, using sensors such as radiometer, lidar and Dopplerized mm-  
250 wave radar, in order to provide vertical profiles of the main cloud variables (e.g., LWC and  
251 IWC) (Hogan et al., 2006). In the Cloudnet observation, particularly, LWC is measured by  
252 radiometer with a spatial resolution of  $\sim 50$  m in the vertical direction and a temporal  
253 resolution of 30 seconds. The retrieval of IWC is performed by using radar reflectivity and  
254 lidar backscatter in the Cloudnet observation with a spatial resolution of  $\sim 10$  m in the  
255 vertical direction and a temporal resolution of 30 seconds as described in Donovan et al.  
256 (2001), Donovan and Lammeren (2001), Donovan (2003) and Tinel et al. (2005). In the  
257 retrieval, the lidar signal and radar reflectivity profiles are combined and inverted using a  
258 combined lidar/radar equation as a function of the light extinction coefficient and radar  
259 reflectivity. The combined equation is detailed in Donovan and Lammeren (2001). In the  
260 Cloudnet data, LWC data with the coarser spatial resolution than IWC data are interpolated  
261 to observation locations of IWC data, and IWP and LWP data are obtained from these IWC  
262 and interpolated LWC data, respectively. The Cloudnet observation data including these  
263 IWC, LWC, IWP and LWP data are provided to the public with a temporal resolution of  
264 30 seconds in a continuous manner. This study utilizes these publicized Cloudnet data.

265 On average, the bottom and top of the observed clouds, which are measured by radar  
266 and lidar in the Cloudnet observation, are at  $\sim 400$  m and  $\sim 3$  km in altitude, respectively.  
267 The simulation of the observed system or case, i.e., the control run, is performed three-  
268 dimensionally over the red rectangle and the period between 02:00 and 10:00 LST on  
269 March 29<sup>th</sup>, 2017. The horizontal domain adopts a 100-m resolution for the control run. The  
270 length of the domain in the horizontal directions is 50 km. The length of the domain in the

271 vertical direction is  $\sim 5$  km and the resolution for the vertical domain gets coarsened with  
272 height from  $\sim 5$  m just above the surface to  $\sim 150$  m at the model top as detailed in the  
273 supplement. Reanalysis data, which are produced by Met Office Unified Model (Brown et  
274 al., 2012) every 6 hours on a  $0.11^\circ \times 0.11^\circ$  grid, provide potential temperature, specific  
275 humidity, and wind as initial and boundary conditions, which represent synoptic-scale  
276 environment, for the control run. The control run employs an open lateral boundary  
277 condition. Figure 2a shows the vertical distribution of the domain-averaged potential  
278 temperature and humidity in those reanalysis data at the first time step. A neutral, mixed  
279 layer is between the surface and 1 km in altitude as an initial condition (Figure 2a). Figure  
280 2b shows the time evolution of the domain-averaged large-scale subsidence or downdraft  
281 in the reanalysis data and at the model top. This large-scale subsidence is imposed on the  
282 control run as a part of background wind fields and interacts with updrafts and downdrafts  
283 generated by relatively small-scale processes including those associated with clouds. The  
284 large-scale subsidence gradually reduces with time (Figure 2b). Figure 2c shows the time  
285 evolution of the domain-averaged surface temperature in the reanalysis data. This evolution  
286 of the surface temperature is strongly controlled by the sea surface temperature considering  
287 that a large portion of the red-rectangle domain is accounted for by the ocean (Figure 1).  
288 Due to the sunrise, the surface temperature starts to increase more rapidly around 08:00  
289 LST (Figure 2c).

290 The properties of cloud condensation nuclei (CCN) such as the number concentration,  
291 size distribution and composition are measured in the domain (Tunved et al., 2013; Jung et  
292 al., 2018). The measurement of the CCN concentration has been carried out at the location  
293 marked by a dot in Figure 1, using the commercial droplet measurement technologies CCN  
294 counter with one column (CCNC-100), managed by the Korea Polar Research Institute,  
295 since year 2007. The CCNC-100 measures the CCN concentration at supersaturations of  
296 0.2, 0.4, 0.6, 0.8 and 1% (Jung et al., 2018). The aerosol number size distribution is  
297 observed using a closed-loop differential mobility particle sizer (DMPS). The DMPS  
298 charges aerosol particles and exposing them into an electric field, which causes them to  
299 experience a force proportional to their electrical mobility, resulting in their classification  
300 according to size (Tunved et al., 2013). Aerosol composition is measured using aerosol

301 mass spectrometry (AMS). The AMS measures the composition by vaporizing and ionizing  
302 aerosol particles.

303 The measurement indicates that on average, aerosol particles are an internal mixture  
304 of 70 % ammonium sulfate and 30 % organic compound. This mixture is assumed to  
305 represent aerosol chemical composition over the whole domain and simulation period for  
306 this study. The observed and averaged concentration of aerosols acting as CCN is  $\sim 200$   
307  $\text{cm}^{-3}$  over the simulation period between 02:00 and 10:00 LST on March 29<sup>th</sup>, 2017. Note  
308 that the average of a variable with respect to time in the rest of this paper is performed over  
309 this period between 02:00 and 10:00 LST, unless otherwise stated.  $200 \text{ cm}^{-3}$  as the averaged  
310 concentration of aerosols acting as CCN is interpolated into all of grid points immediately  
311 above the surface at the first time step.

312 This study does not take into account aerosol effects on radiation before aerosol is  
313 activated, since no significant amount of radiation absorbers is found in the mixture. Based  
314 on observation, the size distribution of aerosols acting as CCN is assumed to be a tri-modal  
315 log-normal distribution (Figure 3). The shape of distribution, which is a tri-modal log-  
316 normal distribution, as shown in Figure 3 is applied to the size distribution of aerosols  
317 acting as CCN in all parts of the domain during the whole simulation period. The assumed  
318 shape in Figure 3 is obtained by performing the average on the observed size distribution  
319 parameters (i.e., modal radius and standard deviation of each of nuclei, accumulation and  
320 coarse modes, and the partition of aerosol number among those modes) over the simulation  
321 period. Note that although these parameters or the shape of aerosol size distribution does  
322 not vary, associated aerosol concentrations vary over the simulation domain and period via  
323 processes as described in Section 2.1. This study takes an assumption that the interpolated  
324 CCN concentrations do not vary with height in a layer between the surface and the  
325 planetary boundary layer (PBL) top around 1 km in altitude at the first time step, following  
326 the previous studies such as Gras (1991), Jaenicke (1993) and Seinfeld and Pandis (1998).  
327 However, above the PBL top, they are assumed to decrease exponentially with height at  
328 the first time step, based on those previous studies, although the shape of size distribution  
329 and composition do not change with height. It is assumed that the properties of INP and  
330 CCN are not different except for concentrations. The concentration of aerosols acting as  
331 CCN is assumed to be 100 times higher than that acting as INP over grid points at the first

332 time step based on a general difference in concentrations between CCN and INP  
333 (Pruppacher and Klett, 1978). Hence, the concentration of aerosols acting as INP at the  
334 first time step is  $2 \text{ cm}^{-3}$  in the control run. This assumed concentration of aerosols acting  
335 as INP is higher than usual (Seinfeld and Pandis, 1998). However, Hartmann et al. (2021)  
336 observed the INP concentration that was at the same order of magnitude as assumed here  
337 in the Svalbard area when strong dust events occur, meaning that the assumed INP  
338 concentration is not that unrealistic.

339 To examine effects of aerosols on mixed-phase clouds, the control run is repeated by  
340 increasing the concentration of aerosols by a factor of 10. In the repeated (control) run, the  
341 initial concentrations of aerosols acting as CCN and INP at grid points immediately above  
342 the surface are 2000 (200) and  $20 \text{ (2) cm}^{-3}$ , respectively. Reflecting these concentrations in  
343 the simulation name, the control run is referred to as “the 200\_2 run” and the repeated run  
344 is referred to as “the 2000\_20 run”. To isolate effects of aerosols acting as CCN (INP) on  
345 mixed-phase clouds, the control run is repeated again by increasing the concentration of  
346 aerosols acting as CCN (INP) only but not INP (CCN) by a factor of 10. In this repeated  
347 run with the increase in the concentration of aerosols acting as CCN (INP), the initial  
348 concentrations of aerosols acting as CCN and INP at grid points immediately above the  
349 surface are 2000 (200) and  $2 \text{ (20) cm}^{-3}$ , respectively. Reflecting this, the repeated run is  
350 referred to as “the 2000\_2 (200\_20) run”.

351

### 352 **2.2.2 Additional simulations**

353

354 To isolate impacts of ice processes on the adopted case and its interactions with aerosols,  
355 the 200\_2 and 2000\_2 runs are repeated by removing ice processes. These repeated runs  
356 are referred to as the 200\_0 and 2000\_0 runs. In the 200\_0 and 2000\_0 runs, all  
357 hydrometeors (i.e., ice crystals, snow, graupel, and hail), phase transitions (e.g., deposition  
358 and sublimation) and aerosols (i.e., INP) which are associated with ice processes are  
359 removed. Hence, in these runs, only droplets (i.e., cloud liquid), raindrops, associated phase  
360 transitions (e.g., condensation and evaporation) and aerosols acting as CCN are present,  
361 regardless of temperature. Stated differently, these noise runs simulate the warm-cloud  
362 counterpart of the selected mixed-phase cloud system. Via comparisons between a pair of

363 the 200\_2 and 2000\_2 runs and a pair of the 200\_0 and 2000\_0 runs, the role of ice  
364 processes in the differentiation between mixed-phase and warm clouds is to be identified.  
365 Along with this identification, the role of the interplay between ice crystals and droplets in  
366 the development of the selected mixed-phase cloud system and its interactions with  
367 aerosols is to be isolated.

368 As detailed in Sections 3.1.4 and 3.2.2 below, the test of ICNC/CDNC as a general  
369 factor requires more simulations to see impacts of ICNCavg/CDCNavg on clouds and their  
370 interactions with aerosols. Here, ICNCavg and CDNCavg represent the average ICNC and  
371 CDNC over grid points and time steps with non-zero ICNC and CDNC, respectively.  
372 ICNCavg/CDNCavg represents overall ICNC/CDNC over the domain and simulation  
373 period. To respond to this requirement, the 200\_0.07, 2000\_0.07 and 200\_0.7 runs are  
374 performed and their details are given in Sections 3.1.4 and 3.2.2. In addition, all the  
375 simulations above are repeated by turning off radiative processes and Section 3.3 provides  
376 the details of these repeated simulations. These repeated runs are the 200\_2\_norad,  
377 2000\_20\_norad, 2000\_2\_norad, 200\_20\_norad, 200\_0\_norad, 2000\_0\_norad,  
378 200\_0.07\_norad, 2000\_0.07\_norad and 200\_0.7\_norad runs. Moreover, based on the  
379 argument in Section 4.2, the 4000\_45, 13\_0.1, 4000\_1.8 and 12\_0.0035 runs are performed  
380 and details of these runs are provided in Section 4.2. Some of the simulations are  
381 summarized in Table 1 for better clarification with a brief description of their configuration.

382

### 383 **3. Results**

384

#### 385 **3.1 The 200\_2 run vs. the 200\_0 run**

386

##### 387 **3.1.1 Model validation**

388

389 This study adopts the Cloudnet observation, which has been used to assess cloud  
390 simulations as in Illingworth et al. (2007) and Hansen et al. (2018), to evaluate the 200\_2  
391 run. Simulated LWP and IWP, as shown in Figure 4 and Table 2, are compared to the  
392 observed LWP and retrieved IWP in the Cloudnet data, respectively. The average LWP  
393 over all time steps and grid columns for the period between 02:00 and 10:00 LST on March

394 29<sup>th</sup>, 2017 is  $1.23 \text{ g m}^{-2}$  in the 200\_2 run and  $1.12 \text{ g m}^{-2}$  in the Cloudnet observation. The  
395 average IWP over all time steps and grid columns over the period is  $31.94 \text{ g m}^{-2}$  in the  
396 200\_2 run and  $29.10 \text{ g m}^{-2}$  in the retrieval. Cloud-bottom height, which is averaged over  
397 grid columns and time steps with non-zero cloud-bottom height over the period, is 420 m  
398 in the 200\_2 run and 440 m in the Cloudnet observation. Cloud-top height, which is  
399 averaged over grid columns and time steps with non-zero cloud-top height over the period,  
400 is 3.5 km in the 200\_2 run and 3.3 km in the Cloudnet observation. Each of LWP, cloud-  
401 bottom and -top heights shows an  $\sim 10\%$  difference between the 200\_2 run and observation.  
402 IWP also shows an  $\sim 10\%$  difference between the 200\_2 run and the retrieval. Thus, the  
403 200\_2 run is considered performed reasonably well for these variables.

404 To provide additional information of cloud development, Figure 5 shows the time  
405 evolution of the simulated and observed cloud-top and bottom heights, simulated and  
406 retrieved IWP and simulated and observed LWP together with the evolution of the  
407 simulated surface sensible and latent-heat fluxes; the simulated evolutions in Figure 5 are  
408 from the 200\_2 run. This is based on the fact that the cloud-top and bottom heights, IWP  
409 and LWP are considered a good indicative of cloud development and the surface fluxes are  
410 considered important parameters controlling the overall development of clouds. The cloud-  
411 top height increases between 02:00 and  $\sim 05:00$  LST and after  $\sim 05:00$  LST, it reduces  
412 gradually. The cloud-bottom height decreases between 02:00 and  $\sim 05:00$  LST and after  
413  $\sim 05:00$  LST, it does not change much. IWP and LWP show an overall increase between  
414 02:00 and  $\sim 05:30$  LST to reach its peak around 05:30 LST and then an overall decrease.  
415 The surface fluxes reduce with time, although the reduction rate of the fluxes starts to  
416 decrease around 08:00 LST in association with the rapid increase in the surface temperature  
417 which starts around 08:00 LST as shown in Figure 2c.

418 The time- and domain-averaged IWP is  $\sim$ one order of magnitude greater than LWP, and  
419 the time- and domain-averaged IWC is  $\sim$ one order of magnitude greater than LWC in the  
420 200\_2 run (Figure 4 and Table 2). For the sake of simplicity, the averaged IWC over the  
421 averaged LWC is denoted by IWC/LWC, and the averaged IWP over the averaged LWP  
422 is by IWP/LWP, henceforth. IWC/LWC is 26.28 and IWP/LWP is 25.96 in the 200\_2 run.  
423 Since IWP and LWP are vertically integrated IWC and LWC over the vertical domain,  
424 respectively, the qualitative nature of differences between IWC and LWC is not much

425 different from that between IWP and LWP. Hence, mentioning both a pair of IWC and  
426 LWC and that of IWP and LWP is considered redundant, and mentioning either a pair of  
427 IWC and LWC or that of IWP and LWP enhances the readability. Henceforth, IWC and  
428 LWC are chosen to be mentioned in text, although all of IWC, LWC, IWP and LWP are  
429 displayed in Tables 2 and 3.

430 Choi et al. (2014) and Zhang et al. (2019) have obtained the supercooled cloud fraction  
431 (SCF), which is basically the ratio of LWC to the sum of LWC and IWC and denoted by  
432  $LWC/(LWC+IWC)$ , using satellite- and ground-observed data collected over the period of  
433  $\sim 1$  year to  $\sim 5$  years. Choi et al. (2014) have shown that SCF is as low as  $\sim 0.01$  for the  
434 temperature range between  $-16$  and  $-33$  °C. Zhang et al. (2019) have also shown that SCF  
435 is as low as  $\sim 0.03$  for the same temperature range, although the occurrence of SCF of  $\sim 0.03$   
436 or lower is rare. Note that the average air temperature immediately below the cloud base  
437 and above the cloud top over the simulation period is  $-16$  and  $-33$  °C, respectively, in the  
438 200\_2 run, and SCF in the 200\_2 run is 0.04. Hence, based on Choi et al. (2014) and Zhang  
439 et al. (2019), we believe that SCF in the 200\_2 run is observable and thus not that  
440 unrealistic, although it may not occur frequently.

441

### 442 **3.1.2 Microphysical processes, sedimentation and entrainment**

443

444 To understand process-level mechanisms that control the results, microphysical processes  
445 are analyzed. As indicated by Ovchinnikov et al. (2011), in clouds with weak precipitation,  
446 a high-degree correlation is found between IWC and deposition or between LWC and  
447 condensation, considering that deposition is the source of IWC and condensation is the  
448 source of LWC. In the 200\_2 run, the average surface precipitation rate over the simulation  
449 period is  $\sim 0.0020$  mm hr<sup>-1</sup>, which can be considered weak. Hence, in this case,  
450 condensation is considered a proxy for LWC, and deposition is a proxy for IWC. Based on  
451 this, to gain a process-level understanding of microphysical processes that control the  
452 simulated LWC and IWC, condensation and deposition are analyzed.

453 As seen in Figure 6 and Table 2, the average deposition rate is  $\sim$ one order of magnitude  
454 greater than condensation rate in the 200\_2 run, leading to much greater IWC than LWC  
455 in the 200\_2 run. This is in contrast to the situation in the case of mixed-phase

456 stratocumulus clouds, which were located in a midlatitude region, in Lee et al. (2021). In  
457 that case, the average IWC and LWC are at the same order of magnitude. For the sake of  
458 brevity, the case in Lee et al. (2021) is referred to as “the midlatitude case”, while the case  
459 of mixed-phase clouds, which is adopted by this study, in the Svalbard area is referred to  
460 “the polar case”, henceforth. In the midlatitude case, IWC/LWC is 1.55, which is ~ one  
461 order of magnitude smaller than that in the polar case.

462 Warm clouds in the 200\_0 run shows that the time- and domain-averaged condensation  
463 rate that is lower than the time- and the domain-averaged sum of condensation and  
464 deposition rates in the 200\_2 run (Figure 6 and Table 2). This leads to a situation where  
465 warm clouds in the 200\_0 run shows the time- and domain-averaged LWC that is lower  
466 than the time- and domain-averaged water content (WC), which is the sum of IWC and  
467 LWC, in mixed-phase clouds in the 200\_2 run (Figure 4 and Table 2). This is despite the  
468 fact that LWC in the 200\_0 run is higher than LWC in the 200\_2 run (Figure 4 and Table  
469 2); WC represents the total cloud mass in mixed-phase clouds, while LWC alone represents  
470 the total cloud mass in warm clouds.

471 It should be noted that the average rate of sedimentation of droplets over the cloud  
472 base and simulation period reduces from the 200\_0 run to the 200\_2 run (Table 2). This is  
473 mainly due to the decrease in LWC from the 200\_0 run to the 200\_2 run. The average rate  
474 of sedimentation of ice crystals over the cloud base and simulation period increases from  
475 the 200\_0 run to the 200\_2 run, since sedimentation of ice crystals is absent in the 200\_0  
476 run (Table 2). The average entrainment rate over the cloud top and simulation period  
477 increases from the 200\_0 run to the 200\_2 run (Table 2). Here, entrainment rate is defined  
478 to be the difference between the rate of increase in cloud-top height and the large-scale  
479 subsidence, following Moeng et al. (1999), Jiang et al. (2002), Stevens et al. (2003a and  
480 2003b) and Ackerman et al. (2004). Entrainment tends to reduce the total cloud mass more  
481 in the 200\_2 run than in the 200\_0 run. Thus, entrainment should be opted out when it  
482 comes to mechanisms leading to the increase in the total cloud mass from the 200\_0 run to  
483 the 200\_2 run. Here, the vertical integration of each of condensation and deposition rates  
484 is obtained over each cloudy column in the domain for each of the runs. For the sake of the  
485 brevity, this vertical integrations of condensation and deposition rates are referred to as the  
486 integrated condensation and deposition rates, respectively. Then, each of the integrated



487 condensation and deposition rates is averaged over cloudy columns and the simulation  
488 period. It is found that the average rate of the droplet sedimentation over the cloud base  
489 and simulation period is ~four orders of magnitude smaller than the average integrated  
490 condensation rate in the 200\_2 run (Table 2). The average rate of the ice-crystal  
491 sedimentation over the cloud base and simulation period is ~four orders of magnitude  
492 smaller than the average integrated deposition rate in the 200\_2 run (Table 2). It is also  
493 found that the average rate of the droplet sedimentation over the cloud base and simulation  
494 period is ~five orders of magnitude smaller than that in the average integrated condensation  
495 rate in the 200\_0 run (Table 2). Changes in the average rate of the droplet sedimentation  
496 over the cloud base and simulation period are ~four to five orders of magnitude smaller  
497 than those in the average integrated condensation rate between the 200\_2 and 200\_0 runs  
498 (Table 2). Changes in the average rate of the ice-crystal sedimentation over the cloud base  
499 and simulation period are ~four to five orders of magnitude smaller than those in the  
500 average integrated deposition rate between the 200\_2 and 200\_0 runs (Table 2). Thus,  
501 condensation and deposition, but not the droplet and ice-crystal sedimentation, are main  
502 factors controlling cloud mass, which is represented by LWC and IWC, and the total cloud  
503 mass in the 200\_2 and 200\_0 runs. The variation of cloud mass and the total cloud mass  
504 between the runs are also mainly controlled by condensation and deposition, but not by  
505 droplet and ice-crystal sedimentation. These dominant roles of condensation and  
506 deposition over those of droplet and ice-crystal sedimentation are observed in the  
507 midlatitude case and its warm-cloud counterpart as well.

508

509

### 3.1.3 Hypothesis

510

511 We hypothesized that ICNC/CDNC can be an important factor that determines above-  
512 described differences between the polar and midlatitude cases. Note that both in the polar  
513 and midlatitude cases, pockets of ice particles and those of liquid particles are mixed  
514 together instead of being separated from each other as seen in Figure 4 and Lee et al. (2021).  
515 Remember that ice crystals are more as sources of deposition per a droplet when  
516 ICNC/CDNC is higher. Thus, as ICNC/CDNC increases in a situation where  $q_v > q_{sw}$ , it  
517 is likely that the portion of water vapor, which is deposited onto ice crystals, increases.

518 This is by stealing water vapor, which is supposed to be condensed onto droplets, from  
519 droplets in an air parcel. Here,  $q_v$  and  $q_{sw}$  represent water-vapor pressure and water-vapor  
520 saturation pressure for liquid water or droplets, respectively. As ICNC/CDNC increases in  
521 a situation where  $q_{si} < q_v < q_{sw}$ , the number of ice crystals, which absorb water vapor,  
522 increases per a droplet; here, water vapor absorbed by ice crystals includes that which is  
523 produced by droplet evaporation, and  $q_{si}$  represents water-vapor saturation pressure for ice  
524 water or ice crystals. Thus, as ICNC/CDNC increases, it is likely that the portion of water  
525 vapor, which is deposited onto ice crystals in an air parcel, increases as shown in Lee et al.  
526 (2021). This is aided by the higher capacitance of ice crystals than that of droplets  
527 (Pruppacher and Klett, 1978). Figure 7 shows the time series of the averaged  
528 supersaturation over grid points where deposition occurs in the presence of both droplets  
529 and ice crystals in the 200\_2 run. Figure 7 indicates that on average, supersaturation occurs  
530 for both droplets and ice crystals over those grid points. Hence, on average, the above-  
531 described situation of  $q_v > q_{sw}$  is applicable to deposition when droplets and ice crystals  
532 coexist in the 200\_2 run.

533 ICNC<sub>avg</sub>/CDNC<sub>avg</sub> is 0.22 in the control run (i.e., the 200\_2 run) for the polar case  
534 and 0.019 in the control run for the midlatitude case which is described in Lee et al. (2021).  
535 Henceforth, the control run for the midlatitude case is referred to as the control-midlatitude  
536 run. ICNC<sub>avg</sub>/CDNC<sub>avg</sub> is ~one order of magnitude higher for the polar case than for the  
537 midlatitude case. This is despite the fact that the ratio of the initial number concentration  
538 of aerosols acting as INP to that of acting as CCN is identical between the 200\_2 and  
539 control-midlatitude runs. In addition, identical model, model setup such as vertical  
540 resolutions, and source of reanalysis data are used between the 200\_2 and control-  
541 midlatitude runs. However, there are differences in environmental conditions (e.g.,  
542 temperature), cloud macrophysical variables such as cloud-top height and horizontal  
543 resolutions between the runs. Here, while taking these similarities and differences into  
544 account, we hypothesize that the significant differences in ICNC<sub>avg</sub>/CDNC<sub>avg</sub> between  
545 runs are mainly due to the fact that ice nucleation strongly depends on air temperature  
546 (Pruppacher and Klett, 1978). When supercooling is stronger, in general, more ice crystals  
547 are nucleated for a given group of aerosols acting as INP. The average air temperature  
548 immediately below the cloud base over the simulation period is -16 °C in the 200\_2 run

549 and -5 °C in the control-midlatitude run. The average air temperature immediately above  
550 the cloud top is -33 °C in the 200\_2 run and -15 °C in the control-midlatitude run. Hence,  
551 supercooling is greater and this contributes to the higher ICNCavg/CDNCavg in the polar  
552 case than in the midlatitude case. The higher ICNCavg/CDNCavg is likely to induce more  
553 portion of water vapor to be deposited onto ice crystals in the polar case than in the  
554 midlatitude case. It is hypothesized that this in turn enables IWC/LWC in the 200\_2 run to  
555 be one order of magnitude greater than that in the control-midlatitude run or in the  
556 midlatitude case. Much higher IWC than LWC, which results in a much higher IWC/LWC  
557 in the polar case than in the midlatitude case, in the 200\_2 run overcomes lower LWC in  
558 the 200\_2 run than that in the 200\_0 run, which leads to the greater total cloud mass in the  
559 200\_2 run than in the 200\_0 run (Figure 4 and Table 2). However, IWC whose magnitude  
560 is similar to the magnitude of LWC, which results in a much lower IWC/LWC in the  
561 midlatitude case than in the polar case, in the midlatitude case is not able to overcome  
562 lower LWC in the midlatitude case than that in the midlatitude warm clouds, which leads  
563 to the greater total cloud mass in the midlatitude warm clouds than in the midlatitude case;  
564 here, the midlatitude warm clouds are generated by removing ice processes in the  
565 midlatitude case. This means that associated with higher ICNC/CDNC and IWC/LWC, ice  
566 processes enhance the total cloud mass for the polar case as compared to that for the polar  
567 warm-cloud counterpart. However, in the midlatitude case, associated with lower  
568 ICNC/CDNC and IWC/LWC, ice processes reduce the total cloud mass as compared to  
569 that for the midlatitude warm-cloud counterpart.

570

#### 571 **3.1.4 Role of ICNC/CDNC**

572

573 To test the hypothesis above about the role of ICNC/CDNC in above-described differences  
574 between the polar and midlatitude cases, the 200\_2 run is repeated by reducing  
575 ICNCavg/CDNCavg by a factor of 10. This is done by reducing the concentration of  
576 aerosols acting as INP but not CCN in a way that ICNCavg/CDNCavg is lower by a factor  
577 of 10 in the repeated run than in the 200\_2 run. In this way, this repeated run has  
578 ICNCavg/CDNCavg at the same order of magnitude as that in the control-midlatitude run.  
579 This repeated run is referred to as the 200\_0.07 run. As shown in Figure 8 and Table 2, the

580 200\_0.07 run shows much lower deposition rate and IWC than the 200\_2 run does.  
581 However, as we move from the 200\_2 run to the 200\_0.07 run, the time- and domain-  
582 averaged condensation rate and LWC increases (Figure 8 and Table 2). This is because  
583 reduction in deposition increases the amount of water vapor, which is not consumed by  
584 deposition but available for condensation. Associated with this, in the 200\_0.07 run, the  
585 time- and domain-averaged deposition rate and IWC become similar to the average  
586 condensation rate and LWC, respectively (Figure 8 and Table 2). Hence, IWC/LWC  
587 reduces from 26.28 in the 200\_2 run to 1.05 in the 200\_0.07 run as ICNCavg/CDNCavg  
588 reduces from the 200\_2 run to the 200\_0.07 run. Here, IWC/LWC in the 200\_0.07 run is  
589 similar to that in the midlatitude-control run, which demonstrate that the difference in  
590 ICNC/CDNC is able to explain the difference in IWC/LWC between the polar and  
591 midlatitude cases. It is notable that the reduction in deposition is dominant over the increase  
592 in condensation with the decrease in ICNCavg/CDNCavg. Hence, the sum of condensation  
593 and deposition rates and WC reduce from the 200\_2 run to the 200\_0.07 run. That the sum  
594 of condensation and deposition rates and WC reduce in a way that the sum and WC in the  
595 mixed-phase clouds in the 200\_0.07 run are lower than condensation rate and LWC,  
596 respectively, in the warm clouds in the 200\_0 run is also notable (Figure 8 and Table 2).  
597 This is similar to the situation in the midlatitude case and thus demonstrates that the  
598 different relation between the mixed-phase and warm clouds can be associated with the  
599 difference in ICNC/CDNC between the polar and midlatitude cases.

600 The rate of the sedimentation of ice crystals at the cloud base reduces as  
601 ICNCavg/CDNCavg reduces between the 200\_2 and 200\_0.07 runs, mainly due to  
602 reduction in the ice-crystal mass (Table 2). The rate of droplet sedimentation at the cloud  
603 base increases as ICNCavg/CDNCavg reduces mainly due to increases in droplet mass and  
604 size in association with the increases in LWC (Table 2). The entrainment rate at the cloud  
605 top reduces as ICNCavg/CDNCavg reduces (Table 2). It is found that those changes in the  
606 average rates of the droplet and ice-crystal sedimentation over the cloud base and  
607 simulation period are ~four to five orders of magnitude smaller than those in the average  
608 integrated condensation and deposition rates between the 200\_2 and 200\_0.07 runs (Table  
609 2). The entrainment tends to reduce the total cloud mass or WC less with the reducing  
610 ICNCavg/CDNCavg. Hence, changes in the entrainment counters the decrease in WC with

611 the reducing ICNCavg/CDNCavg between the 200\_2 and 200\_0.07 runs. Here, we see that  
612 changes in the entrainment are not factors that lead to the increase in LWC, and the  
613 decrease in IWC, and eventually the decrease in WC with the reducing  
614 ICNCavg/CDNCavg. The analysis of the sedimentation and entrainment exclude them  
615 from factors inducing above-described differences between the 200\_2 and 200\_0.07 runs.  
616 Instead, this analysis grants confidence in the fact that deposition and condensation, which  
617 are strongly dependent on ICNC/CDNC, are main factors inducing those differences.

618

### 619 **3.2 Aerosol-cloud interactions**

620

621 Comparisons between the 200\_2 and 2000\_20 runs show that with the increasing  
622 concentration of both of aerosols acting as CCN and those as INP, IWC increases but LWC  
623 decreases in the polar case (Figures 9 and Table 2). These decreases in LWC are negligible  
624 as compared to these increases in IWC. Hence, the increases in IWC outweigh the  
625 decreases in LWC, leading to aerosol-induced increases in WC (Figures 9 and Table 2).  
626 To identify roles of specific types of aerosols in these aerosol-induced changes,  
627 comparisons not only between the 200\_2 and 200\_20 runs but also between the 200\_2 and  
628 2000\_2 runs are performed. Comparisons between the 200\_2 and 200\_20 runs show that  
629 the increasing concentration of aerosols acting as INP induces increases in IWC but  
630 decreases in LWC (Figure 9 and Table 2). The magnitudes of these increases and decreases  
631 are similar to those between the 200\_2 and 2000\_20 runs (Figure 9 and Table 2). However,  
632 comparisons between the 200\_2 and 2000\_2 runs show that the increasing concentration  
633 of aerosols acting as CCN induces negligible changes in either IWC or LWC. Thus, CCN-  
634 induced changes in the total cloud mass are negligible, although the increasing  
635 concentration of aerosols acting as CCN induces a slight decrease in IWC, and a slight  
636 increase in LWC (Figure 9 and Table 2). This demonstrates that INP plays a much more  
637 important role than CCN when it comes to the response of the total cloud mass to increasing  
638 aerosol concentrations. However, in the midlatitude case, the increasing concentration of  
639 aerosols acting as CCN generates changes in the mass as significantly as the increasing  
640 concentration of aerosols acting as INP does.

641 To identify roles played by ice processes in aerosol-cloud interactions, a pair of the  
642 200\_0 and 2000\_0 runs are analyzed and compared to the previous four standard  
643 simulations (i.e., the 200\_2, 200\_20, 2000\_2 and 2000\_20 runs). The CCN-induced  
644 increases in LWC in those noise runs are much greater than the CCN-induced changes in  
645 WC in the 200\_2 and 2000\_2 runs (Figure 9 and Table 2). However, these CCN-induced  
646 increases in LWC in the noise runs are smaller than the INP-induced increases in WC in  
647 the 200\_2 and 200\_20 runs (Figure 9 and Table 2). This is different from the midlatitude  
648 case where changes in the total cloud mass, whether they are induced by the increasing  
649 concentration of aerosols acting as CCN or INP, in the mixed-phase clouds are much lower  
650 than those CCN-induced changes in the warm clouds.

651

### 652 **3.2.1 Deposition, condensation, sedimentation and entrainment**

653

654 The CCN-induced increases in condensation rates and decreases in deposition rates are  
655 negligible. This leads to the CCN-induced negligible increases in LWC and negligible  
656 decreases in IWC between the 200\_2 and 2000\_2 runs (Figure 9 and Table 2). However,  
657 between the 200\_2 and 200\_20 runs, rather the significant INP-induced increases are in  
658 deposition rate, leading to the significant INP-induced increases in IWC (Figure 9 and  
659 Table 2). Between the 200\_2 and 200\_20 runs, INP-induced decreases in condensation  
660 rate are negligible, leading to the negligible INP-induced decreases in LWC, as compared  
661 to the INP-induced increases in deposition rate and IWC (Figure 9 and Table 2). With the  
662 increasing concentration of aerosols acting as INP from the 200\_2 run to the 200\_20 run,  
663 the sedimentation of ice crystals at the cloud base decreases (Table 2). This is mainly due  
664 to decreases in the size of ice crystals in association with increases INP and resultant  
665 increases in ICNC. In Figure 10a, we see that the number concentration of ice crystals with  
666 diameters smaller and larger than ~40 micron increases and decreases, respectively, as we  
667 move from the 200\_2 run to the 200\_20 run, which indicate a shift of the sizes of ice  
668 crystals to smaller ones. From the 200\_2 run to the 200\_20 run, the sedimentation of  
669 droplets at the cloud base decreases as shown in Table 2, mainly due to decreases in LWC.  
670 Figure 10b shows that the number concentration of drops decreases throughout almost all  
671 parts of the size range from the 200\_2 run to the 200\_20 run, which indicates a negligible

672 shift in the drop size but a reduction in LWC. It is found that changes in the average rates  
673 of the droplet and ice-crystal sedimentation over the cloud base and simulation period are  
674 ~three to four orders of magnitude smaller than those in the average integrated  
675 condensation and deposition rates between the 200\_2 and 200\_20 runs (Table 2). From the  
676 200\_2 run to the 200\_20 run, the entrainment at the cloud top increases (Table 2). Hence,  
677 the entrainment reduces WC less in the 200\_2 run than in the 200\_20 run. Here, we see  
678 that changes in entrainment and the sedimentation are not factors that we have to focus on  
679 to explain the changes in LWC, IWC and WC between the 200\_2 and 200\_20 runs.

680 In the warm clouds in the 200\_0 and 2000\_0 runs, the CCN-induced increases in  
681 condensation rate occur, leading to those in LWC (Figure 9 and Table 2). However, the  
682 CCN-induced increases in condensation rate in the warm clouds associated with the polar  
683 case are lower than the INP-induced increases in deposition rate in the polar case (Table  
684 2). This contributes to aerosol-induced smaller changes in the total cloud mass in the polar  
685 warm clouds than in the polar mixed-phase clouds. The sedimentation of droplets at the  
686 cloud base reduces and the entrainment at the cloud top increases from the 200\_0 run to  
687 2000\_0 run (Table 2). The increasing concentration of aerosols acting as CCN induces  
688 increases in CDNC and decreases in the droplet size, leading to the reduction in the droplet  
689 sedimentation from the 200\_0 run to 2000\_0 run. The entrainment counters the CCN-  
690 induced increases in LWC from the 200\_0 run to 2000\_0 run. Hence, the entrainment is  
691 not a factor which induces the CCN-induced increases in LWC between the 200\_0 and  
692 2000\_0 runs. As seen in Table 2, the changes in the sedimentation rate is ~three orders of  
693 magnitude smaller than those in the integrated condensation rate between the 200\_0 and  
694 2000\_0 runs. Hence, it is not the sedimentation but condensation that we have to look at to  
695 explain changes in LWC or WC between the 200\_0 and 2000\_0 runs.

696

### 697 **3.2.2 Understanding differences between the polar and midlatitude cases**

698

699 Roughly speaking, the CCN-induced changes in LWC via CCN-induced changes in  
700 autoconversion of droplets are proportional to LWC that changing CCN affect, and INP-  
701 induced changes in IWC via INP-induced changes in autoconversion of ice crystals are  
702 proportional to IWC that changing INPs affect (e.g., Dudhia, 1989; Murakami, 1990; Liu

703 and Daum, 2004; Morrison et al., 2005, 2009 and 2012; Lim and Hong, 2010; Mansell et  
704 al. 2010; Kogan, 2013; Lee and Baik, 2017). This is for given environmental conditions  
705 (e.g., temperature and humidity) and given CCN- or INP-induced changes in microphysical  
706 factors such as sizes and number concentrations of droplets or ice crystals. Hence, in the  
707 polar case, with a given much lower LWC than IWC, the changing concentration of  
708 aerosols acting as CCN is likely to induce smaller changes in the given LWC via CCN  
709 impacts on the droplet autoconversion. This is as compared to changes in the given IWC  
710 which are induced by the changing concentration of aerosols acting as INP and thus  
711 changing ice-crystal autoconversion.

712 The smaller changes in the given LWC are related to changes in CDNC. These changes  
713 in CDNC are initiated by those in droplet autoconversion. The larger changes in the given  
714 IWC are related to changes in ICNC. These changes in ICNC are initiated by those in ice-  
715 crystal autoconversion. Changes in integrated droplet surface area, which are induced by  
716 those in CDNC, initiate those in the given LWC. Changes in integrated ice-crystal surface  
717 area, which are induced by those in ICNC, initiate those in the given IWC. Remember that  
718 condensation occurs on droplet surface and thus droplets act as a source of condensation,  
719 and deposition occurs on ice-crystal surface and thus ice crystals act as a source of  
720 deposition. Hence, those changes in CDNC and associated integrated droplet surface area  
721 can lead to changes in condensation and thus feedbacks between condensation and updrafts,  
722 while those changes in ICNC and associated integrated ice-crystal surface area can lead to  
723 changes in deposition and thus feedbacks between deposition and updrafts. The smaller  
724 CCN-induced changes in LWC involve changes in CDNC and associated smaller changes  
725 in condensation and feedbacks between condensation and updrafts in the polar case. This  
726 is as compared to changes in deposition and feedbacks between deposition and updrafts  
727 which are associated with the INP-induced changes in ICNC and the related larger INP-  
728 induced changes in IWC in the polar case. The smaller CCN-induced changes in LWC  
729 involve smaller changes in water vapor that is consumed by droplets in the polar case. The  
730 larger INP-induced changes in IWC involve larger changes in water vapor that is consumed  
731 by ice crystals in the polar case. This leaves the CCN-induced smaller changes in the  
732 amount of water vapor available for deposition, which induce the smaller CCN-induced  
733 changes in IWC in the polar case. This is as compared to the INP-induced changes in the



734 amount of water vapor which is available for condensation and associated changes in LWC  
735 in the polar case.

736 The lower LWC in the polar warm clouds than IWC in the polar case contributes to the  
737 INP-induced greater changes in IWC than the CCN-induced changes in LWC in the polar  
738 warm clouds. The lower LWC in the polar case than that in the polar warm clouds  
739 contributes to the CCN-induced greater changes in LWC in the polar warm clouds than  
740 those in LWC and subsequent changes in IWC in the polar case.

741 In contrast to the situation in the polar case, in the midlatitude case, remember that a  
742 given LWC is at the same order of magnitude of IWC. Hence, the CCN- induced changes  
743 in LWC and subsequent changes in IWC are similar to the INP-induced changes in IWC  
744 and subsequent changes in LWC. The greater LWC in the midlatitude warm cloud than  
745 both of LWC and IWC in the midlatitude case contributes to the greater CCN-induced  
746 changes in LWC in the midlatitude warm cloud. This is as compared to either the CCN-  
747 induced changes in LWC and subsequent changes in IWC or the INP-induced changes in  
748 IWC and subsequent changes in LWC in the midlatitude case.

749 To confirm above-described mechanisms in this section, which explain different  
750 aerosol-cloud interactions between the polar and midlatitude cases, the 200\_0.07 run is  
751 repeated by increasing INP by a factor of 10 in the PBL at the first time step. This repeated  
752 run is referred to as “the 200\_0.7 run. Then, the 200\_0.07 run is repeated again by  
753 increasing CCN by a factor of 10 in the PBL at the first time step. This repeated run is  
754 referred to as the 2000\_0.07 run. These repeated runs are to see the response of IWC and  
755 LWC to the increasing concentration of aerosols acting as INP and CCN. This is when  
756 IWC and LWC are at the same order of magnitude and lower in mixed-phase clouds than  
757 LWC in the warm-cloud counterpart as in the 200\_0.07 run and midlatitude case.  
758 Comparisons between the 200\_0.07, 200\_0.7 and 2000\_0.07 runs show that the INP-  
759 induced changes in IWC and LWC are similar to the CCN-induced changes in IWC and  
760 LWC, respectively, as in the midlatitude case (Figure 9 and Table 2). These comparisons  
761 also show that the CCN-induced changes in LWC in the polar warm cloud are greater  
762 (Figure 9 and Table 2). This is as compared to either the CCN-induced changes in LWC  
763 and subsequent changes in IWC between the 200\_0.07 and 2000\_0.07 runs or the INP-  
764 induced changes in IWC and subsequent changes in LWC between the 200\_0.07 and

765 200\_0.7 runs (Figure 9 and Table 2). These comparisons demonstrate that differences in  
766 ICNC/CDNC play a critical role in differences in aerosol-cloud interactions between the  
767 polar and midlatitude cases, considering that differences in ICNC/CDNC between the  
768 200\_2 and 200\_0.07 runs are at the same order of magnitude of those between the cases.

769

### 770 **3.3 Radiation**

771

772 Studies (e.g., Ovchinnikov et al., 2011; Possner et al., 2017; Solomon et al., 2018) have  
773 focused on radiative cooling and subsequent changes in stability and dynamics as a primary  
774 driver for the development of mixed-phase stratocumulus clouds and aerosol-induced  
775 changes in LWC and IWC in those clouds. Motivated by these studies, to isolate the role  
776 of radiative processes in cloud development and aerosol impacts on LWC and IWC, all of  
777 the simulations above are repeated by turning off radiative processes. In these repeated  
778 runs, radiative fluxes over the whole domain and simulation period are zero. The basic  
779 summary of results from these repeated runs is given in Table 3. As seen in comparisons  
780 between Tables 2 and 3, the qualitative nature of results, which are mainly about  
781 differences in IWC/LWC, the relative importance of the impacts of INP on IWC and LWC  
782 as compared to those impacts of CCN, and how warm and mixed-phase clouds are related  
783 between the polar and midlatitude cases, in this study does not vary with whether radiative  
784 processes exist or not. This demonstrates that ICNC, CDNC, deposition and condensation  
785 but not radiative processes drive results in this study.

786

## 787 **4. Discussion**

788

### 789 **4.1 Examination of the role of ICNC/CDNC in IWC/LWC in 200\_2, 790 2000\_20, 2000\_2, 200\_20, 200\_0.07, 2000\_0.07 and 200\_0.7 runs**

791

792 So far, comparisons between the set of the 200\_2, 2000\_20, 2000\_2 and 200\_20 runs for  
793 the polar case and the other set of the 200\_0.07, 2000\_0.07 and 200\_0.7 runs, which  
794 represents the midlatitude case, have been mainly utilized to understand the role of  
795 ICNC/CDNC. However, even when it comes to all the runs in both the sets, differences in

796 ICNCavg/CDNCavg and IWC/LWC are shown among them (Tables 1 and 2). For more  
797 robust examination of particularly the role of ICNC/CDNC in IWC/LWC, which is  
798 basically about the increase and decrease in ICNC/CDNC inducing the increase and  
799 decrease in IWC/LWC, respectively, as identified from the comparison between the 200\_2  
800 and 200\_0.07 runs in Section 3.1.4, all the runs in the sets are utilized by ordering them as  
801 shown in Table 4. This ordering is done in a way that as we move from the first run in the  
802 first row to the last run in the last row of Table 4, ICNCavg/CDNCavg increases. Overall,  
803 with increasing ICNCavg/CDNCavg, IWC/LWC increases in Table 4 as also seen in Figure  
804 11 that shows IWC/LWC as a function of ICNCavg/CDNCavg based on Table 4. This is  
805 despite the fact that the increase in IWC/LWC is highly non-linear in terms of the increase  
806 in ICNCavg/CDNCavg as seen in the percentage increases, and a decrease in IWC/LWC  
807 is seen with an increase in ICNCavg/CDNCavg from the 2000\_20 run to the 200\_2 run  
808 (Table 4 and Figure 11); this high-degree non-linearity in the increase in IWC/LWC is  
809 associated with the fact that interactions between cloud microphysical, thermodynamic and  
810 dynamic processes are well known to be highly non-linear. Hence, overall, findings  
811 regarding the role of ICNC/CDNC in IWC/LWC from the comparison between the 200\_2  
812 and 200\_0.07 runs are applicable to all the runs in the sets except for the role between the  
813 2000\_20 and 200\_2 runs. Here, it is notable that the percentage difference in  
814 ICNCavg/CDNCavg is ~9% between the 2000\_20 and 200\_2 runs and the smallest among  
815 those differences in Table 4. The other differences are larger than 80%. Hence, the  
816 percentage difference in ICNCavg/CDNCavg for a pair of the 2000\_20 and 200\_2 runs is  
817 at least ~one order of magnitude smaller than that for the other pairs of the runs in Table 4.  
818 This means that findings from the comparison between the 200\_2 and 200\_0.07 runs are  
819 not suitable to explain the variation of IWC/LWC among clouds when the variation of  
820 ICNC/CDNC is relatively insignificant. According to Table 4, it seems that the variation  
821 of ICNC/CDNC should be greater than a critical value above which those findings are  
822 useful to account for the IWC/LWC variation among clouds.

823       The high-degree non-linearity in the variation of IWC/LWC is epitomized by the 1706  
824 percent increase in IWC/LWC for the 163 percent increase in ICNCavg/CDNCavg from  
825 the 200\_0.7 run to the 2000\_2 run. This 1706 percent increase in IWC/LWC is induced by  
826 increases in both the initial number concentrations of CCN and INP between the runs

827 (Table 1). In other transition from a simulation in a row to that in the next row in Table 4,  
828 there are decreases in both the initial number concentrations of CCN and INP, or there is  
829 either a change in the initial number condensation of CCN or INP. When either the initial  
830 concentration of CCN or INP changes in the transition, less than a 100% increase in  
831 IWC/LWC is shown. The decreases in both the initial number concentrations of CCN and  
832 INP, which are from the 2000\_20 run to the 200\_2 run, result in the decrease in IWC/LWC.  
833 Hence, depending on how the initial number concentrations of CCN and INP change, the  
834 magnitude and sign of the change in IWC/LWC can vary substantially.

835

#### 836 **4.2 Role of a given ICNC/CDNC in IWC/LWC for different concentrations of** 837 **aerosols acting as INP and CCN**

838

839 Simulations which are compared in Section 4.1 and shown in Table 4 have not only  
840 different ICNCavg/CDNCavg but also the different number concentrations of aerosols  
841 acting as CCN and INP at the first time step (Table 1). To better isolate particularly the  
842 role of ICNC/CDNC in IWC/LWC, we need to show that results in Section 4.1 are valid  
843 regardless of the variation of the number concentration of aerosols. For this need, we focus  
844 on the 200\_2 and 200\_0.07 runs, since the primary understanding of the role of  
845 ICNC/CDNC in IWC/LWC comes from the comparison between these runs as described  
846 in Section 3.1.4. To fulfill the need, each of these runs are repeated by varying the number  
847 concentration of aerosols acting as CCN and INP in a way that ICNCavg/CDNCavg does  
848 not vary (Tables 1 and 5). The 4000\_45 and 13\_0.1 runs are the repeated 200\_2 run, and  
849 the 4000\_1.8 and 12\_0.0035 runs are the repeated 200\_0.07 run (Tables 1 and 5). The set  
850 of the 200\_2, 4000\_45 and 13\_0.1 runs is referred to as the polar set, and that of the  
851 200\_0.07, 4000\_1.8 and 12\_0.0035 runs is referred to as the midlatitude set in this section.  
852 Among the three runs in each of the sets, less than 4% variation of IWC/LWC is shown  
853 (Table 5). This less-than-4% variation is so small that the start contrast in IWC/LWC  
854 between the 200\_2 and 200\_0.07 runs as discussed in Section 3.1.4 is also shown between  
855 the polar and midlatitude sets (Table 5). Hence, the role of the difference in a given  
856 ICNC/CDNC in the difference in IWC/LWC between the 200\_2 and 200\_0.07 runs as  
857 described in Section 3.1.4 is considered robust to the varying concentration of aerosols.

858

859 **4.3 Role of environmental factors, sedimentation, aerosol sources and**  
860 **advection**

861

862 This study picks ICNC/CDNC as an important factor which differentiates IWC/LWC and  
863 interactions among clouds, aerosols and ice processes in the polar case from those in the  
864 midlatitude case. However, this does not mean that no other potential factors, which can  
865 explain the variation of IWC/LWC and interactions among clouds, aerosols and ice  
866 processes between different clouds, exist. For example, differences in environmental  
867 factors (e.g., stability and wind shear) between those different clouds can have an impact  
868 on the variation. Particularly, differences in stability and wind shear can initiate those in  
869 the dynamic development of turbulence. Then, this subsequently induces differences in the  
870 microphysical and thermodynamic development of clouds, IWC/LWC and interactions  
871 among clouds, aerosols and ice processes. Hence, factors such as stability and wind shear  
872 can have different orders of procedures, which involve dynamics, thermodynamics and  
873 microphysics, than ICNC/CDNC in terms of differentiation between different clouds. Thus,  
874 different mechanisms controlling the differentiation can be expected regarding factors such  
875 as stability and wind shear as compared to ICNC/CDNC. The examination of these  
876 different mechanisms among stability, wind shear and ICNC/CDNC deserves future study  
877 for more comprehensive understanding of the differentiation or for an above-mentioned  
878 more fully established general principle explaining the differentiation.

879 Another point to make is that the cases in this study have weak precipitation and the  
880 associated weak sedimentation of ice crystals and droplets. In mixed-phase clouds with  
881 strong precipitation and the sedimentation, they can play roles as important as in-cloud  
882 latent-heat processes in IWC/LWC and interactions among clouds, aerosols and ice  
883 processes. In those clouds with strong precipitation, the sedimentation can take part in the  
884 interplay between ICNC/CDNC and latent-heat processes by affecting cloud mass and  
885 associated ICNC and CDNC significantly, and play a role in the differentiation of  
886 IWC/LWC and interactions among clouds, aerosols and ice processes when it comes to  
887 different cases of mixed-phase clouds. For more generalization of results here as a way to  
888 the more fully established general principle, this potential role of sedimentation needs to

889 be investigated by performing more case studies involving cases with strong precipitation  
890 in the future.

891 It should be emphasized that although this study mentions air temperature as a factor  
892 that affects ICNC/CDNC, ICNC/CDNC can be affected by other factors such as sources of  
893 aerosols acting as INP and those acting as CCN, and/or the advection of those aerosols.  
894 Hence, even for cloud systems that develop with a similar air-temperature condition, for  
895 example, when those systems are affected by different sources of aerosols and/or their  
896 different advection, they are likely to have different ICNC/CDNC, IWC/LWC, relative  
897 importance of impacts of INP on IWC and LWC as compared to those impacts of CCN,  
898 and relation between warm and mixed-phase clouds. Regarding factors, which affect  
899 ICNC/CDNC, such as sources and advection of aerosols together with temperature, it  
900 should be noted that while this study utilizes differences in temperature among those  
901 factors to identify cases exhibiting significant disparities in ICNC/CDNC, its primary  
902 objective does not lie in the role of temperature differences in disparities in ICNC/CDNC,  
903 but in comprehending the inherent role of ICNC/CDNC variations themselves in the  
904 discrepancies observed, for example, in IWC/LWC, across diverse cloud systems.

905

#### 906 **4.4 Mixing of droplets and ice crystals**

907

908 The representation of mixed-phase clouds in our study relies on the assumption of  
909 homogeneously mixed ice and liquid hydrometeors within the model grid cells, a common  
910 approach in many models. However, recent observational studies (e.g., D'Alessandro et al.,  
911 2021; Korolev and Milbrandt, 2022; Schima et al., 2022; Coopman and Tan, 2023) have  
912 shown that in reality, mixed-phase clouds often exhibit inhomogeneous distributions of ice  
913 and liquid, with distinct pockets or regions of each phase. These observations suggest that  
914 the microphysical processes, such as the Wegener-Bergeron-Findeisen process, may be  
915 influenced by this inhomogeneity, potentially leading to differences in cloud dynamics and  
916 feedbacks compared to what is simulated by models assuming the homogeneous mixing.

917 While our study, along with the work of Lee et al. (2021), uses a model-based  
918 approach that assumes the homogeneous mixing, it is important to acknowledge that this  
919 representation may not fully capture the complexity observed in real clouds. The

920 implications of this assumption could affect the accuracy of our simulations, particularly  
921 in scenarios where phase-transition processes in mixed-phase clouds play a significant role.  
922 As such, the results presented should be interpreted with this limitation in mind, and further  
923 work incorporating more detailed representations of inhomogeneous hydrometeor  
924 distributions may be needed to refine our understanding of mixed-phase cloud processes.

925

## 926 **5. Summary and conclusions**

927

928 In this study, a case of mixed-phase stratiform clouds in a polar area, which is referred to  
929 as “the polar case” is compared to that in a midlatitude area, which is referred to as “the  
930 midlatitude case”. This is to gain an understanding of how different ICNC/CDNC plays a  
931 role in making differences in cloud properties, aerosol-cloud interactions and impacts of  
932 ice processes on them between two representative areas (i.e., polar and midlatitude areas)  
933 where mixed-phase stratiform clouds form and develop. Among those cloud properties,  
934 this study focuses on IWC/LWC that plays an important role in cloud radiative properties.  
935 To gain the understanding efficiently, the polar case is chosen in a way to make stark  
936 contrast with the midlatitude case in terms of ICNC/CDNC and IWC/LWC. Although such  
937 polar cases may be uncommon, the stark contrast provides an opportunity to elucidate  
938 mechanisms that control the above-mentioned role of different ICNC/CDNC.

939 Due to lower air temperature, more ice crystals are nucleated, leading to higher  
940 ICNC/CDNC in the polar case than in the midlatitude case. This higher ICNC/CDNC  
941 enables the more efficient deposition of water vapor onto ice crystals in the polar case. This  
942 leads to much higher IWC/LWC in the polar case. The more efficient deposition of water  
943 vapor onto ice crystals enables the polar mixed-phase clouds to have the greater total cloud  
944 mass than the polar warm clouds. However, the less efficient deposition of water vapor  
945 onto ice crystals causes the midlatitude mixed-phase clouds to have less total cloud mass  
946 than the midlatitude warm clouds. With the increasing ICNC/CDNC from the midlatitude  
947 case to the polar case, impacts of CCN and INP on the total cloud mass become less and  
948 more important, respectively.

949 Previous studies on mixed-phase stratocumulus clouds (e.g., Ovchinnikov et al., 2011;  
950 Possner et al., 2017; Solomon et al., 2018) have primarily focused on investigating the

951 impacts of cloud-top radiative cooling, entrainment, and sedimentation of ice particles on  
952 these clouds, as well as their interactions with aerosols. However, there are a scarcity of  
953 studies that specifically examine the role of microphysical interactions, involving  
954 processes such as condensation and deposition, as well as factors like cloud-particle  
955 concentrations, between ice and liquid particles in mixed-phase stratocumulus clouds, and  
956 their interactions with aerosols as performed in this study. Therefore, our study contributes  
957 to a more comprehensive understanding of mixed-phase clouds and their intricate interplay  
958 with aerosols.

959 This study suggests that a microphysical factor, which is ICNC/CDNC, can be a  
960 simplified and useful tool to understand differences among different systems of  
961 stratocumulus clouds in various regions in terms of IWC/LWC and the relative importance  
962 of INP and CCN in aerosol-cloud interactions, and thus to contribute to the development  
963 of general parameterizations of those clouds in various regions for climate models. This  
964 factor can also be a useful tool for a simplified understanding of different roles of ice  
965 processes when mixed-phase clouds are compared to their warm-cloud counterparts in  
966 terms of the cloud development and its interactions with aerosols among those different  
967 systems. It should be noted that warm clouds have been studied much more than mixed-  
968 phase clouds, although mixed-phase clouds play as important roles as warm clouds in the  
969 evolution of climate and its change. This study provides preliminary mechanisms which  
970 differentiate mixed-phase clouds and their interactions with aerosols from their warm-  
971 cloud counterparts, and control the variation of the differentiation in different regions as a  
972 way of improving our understanding of mixed-phase clouds. It should be mentioned that  
973 the efficient way of developing general parameterizations, which are for climate models  
974 and consider all of warm, mixed-phase clouds in various regions and their interactions with  
975 aerosols, can be achieved by just adding those mechanisms to pre-existing  
976 parameterizations of much-studied warm clouds instead of developing brand new  
977 parameterizations from the scratch.

978 This study finds that the relation between ICNC/CDNC and IWC/LWC is highly non-  
979 linear. This high non-linearity is closely linked to how the number concentrations of CCN  
980 and INP, and associated ICNC/CDNC change. For a specific situation where the  
981 ICNC/CDNC variation is relatively small and both the number concentrations of CCN and



982 INP reduce, the increase in ICNC/CDNC can reduce IWC/LWC, although it is found that  
983 as a whole, the increase in ICNC/CDNC enhances IWC/LWC. Hence, mechanisms  
984 identified in this study, especially regarding the use of ICNC/CDNC as a simplified and  
985 useful tool to explain differences in IWC/LWC among different cloud systems, are not  
986 complete and entirely general. In addition, results in this study are from only two cases in  
987 two specific locations in the midlatitude and Arctic regions and the more generalization of  
988 these results in this study merits more case studies over more locations in those regions,  
989 for example, in terms of above-mentioned sedimentation intensity, different factors (e.g.,  
990 environmental factors) other than ICNC/CDNC, different sources and advection of  
991 aerosols, the magnitude of the variation of ICNC/CDNC and the way number  
992 concentrations of CCN and INP vary. Hence, findings particularly about relations between  
993 ICNC/CDNC and IWC/LWC in this study should be considered preliminary ones that  
994 initiate future work to streamline the development of the general parameterizations.

995

996

997

998

999

1000

1001

1002

1003

1004

1005

1006

1007

1008

1009

1010

1011

1012

**1013 Code/Data source and availability**

1014

1015 Our private computer system stores private data such as the model code and output, and  
1016 the CCN data. Upon approval from funding sources, the data will be opened to the public.  
1017 Projects related to this paper have not been finished, thus, the sources prevent the data from  
1018 being open to the public currently. However, if information on the data is needed, contact  
1019 the corresponding author Seoung Soo Lee (slee1247@umd.edu).

1020 The Cloudnet and reanalysis data used in this study are publicly available. The  
1021 Cloudnet data are obtainable at “<https://cloudnet.fmi.fi/search/data>”, while the reanalysis  
1022 data can be obtained by contacting Met Office via “[https://www.metoffice.gov.uk/about-](https://www.metoffice.gov.uk/about-us/contact)  
1023 [us/contact](https://www.metoffice.gov.uk/about-us/contact)”

1024

**1025 Author contributions**

1026 Essential initiative ideas are provided by SSL, CHJ and YJY to start this work. Simulation  
1027 and observation data are analyzed by SSL, CHJ and JU. YZ, JP, MGM and SKS review  
1028 the results and contribute to their improvement. JC provides supports to set up and run  
1029 additional simulations during the review.

1030

**1031 Competing interests**

1032 The authors declare that they have no conflict of interest.

1033

**1034 Acknowledgements**

1035 This study is supported by the National Research Foundation of Korea (NRF) grant funded  
1036 by the Korea government (MSIT) (Nos. NRF2020R1A2C1003215,  
1037 NRF2020R1A2C2011081, NRF2023R1A2C1002367,  
1038 NRF2021M1A5A1065672/KOPRI-PN23011 and 2020R1A2C1013278), and Basic  
1039 Science Research Program through the NRF funded by the Ministry of Education (No.  
1040 2020R1A6A1A03044834).

1041

1042

1043

1044 **References**

1045

1046 Ackerman, A., Kirkpatrick, M., Stevens, D., et al.: The impact of humidity above  
1047 stratiform clouds on indirect aerosol climate forcing, *Science*, 432, 1014–1017,  
1048 <https://doi.org/10.1038/nature03174>, 2004.

1049 Albrecht, B. A.: Aerosols, cloud microphysics, and fractional cloudiness, *Science*, 245,  
1050 1227-1230, 1989.

1051 Bartosiewicz, Y., and Duponcheel, M.: Large eddy simulation: Application to liquid metal  
1052 fluid flow and heat transfer . In: Roelofs, Ferry, *Thermal Hydraulics Aspects of Liquid*  
1053 *Metal Cooled Nuclear Reactors*, Woodhead Publishing, 2018.

1054 Brown, A., Milton, S., Cullen, M., Golding, B., Mitchell, J., and Shelly, A.: Unified  
1055 modeling and prediction of weather and climate: A 25-year journey, *B. Am. Meteorol.*  
1056 *Soc.*, 93, 1865–1877, 2012.

1057 Chen, F., and Dudhia, J.: Coupling an advanced land-surface hydrology model with the  
1058 Penn State-NCAR MM5 modeling system. Part I: Model description and  
1059 implementation, *Mon. Wea. Rev.*, 129, 569–585, 2001.

1060 Choi, Y.-S., Ho, C.-H., Park, C.-E., Storelvmo, T., and Tan, I.: Influence of cloud phase  
1061 composition on climate feedbacks, *J. Geophys. Res.*, 119, 3687–3700,  
1062 doi:10.1002/2013JD020582, 2014.

1063 Choi, Y.-S., Lindzen, R. S., Ho, C.-H., and Kim, J.: Space observations of cold-cloud phase  
1064 change, *Proc. Natl. Acad. Sci. U.S.A.*, 107, 11211–11216, 2010

1065 Chua, X. R., and Ming, Y.: Convective invigoration traced to warm-rain microphysics,  
1066 *Geophys. Res. Lett.*, 47, <https://doi.org/10.1029/2020GL089134>, 2020.

1067 Coopman, Q., and Tan, I.: Characterization of the spatial distribution of the thermodynamic  
1068 phase within mixed-phase clouds using satellite observations, *Geophys. Res. Lett.*, 50,  
1069 e2023GL104977, 2023.

1070 D'Alessandro, J. J., McFarquhar, G. M., Wu, W., Stith, J. L., Jensen, J. B., and Rauber, R.  
1071 M.: Characterizing the occurrence and spatial heterogeneity of liquid, ice, and mixed  
1072 phase low-level clouds over the Southern Ocean using in situ observations acquired  
1073 during SOCRATES, *J. Geophys. Res.*, 126, e2020JD034482, 2021.

1074 Dione, C., Lohou, F., Lothon, M., Adler, B., Babić, K., Kalthoff, N., Pedruzo-Bagazgoitia,

- 1075 X., Bezombes, Y., and Gabella, O.: Low-level stratiform clouds and dynamical  
1076 features observed within the southern West African monsoon, *Atmos. Chem. Phys.*,  
1077 19, 8979–8997, <https://doi.org/10.5194/acp-19-8979-2019>, 2019.
- 1078 Donovan, D. P.: Ice-cloud effective particle size parameterization based on combined lidar,  
1079 radar reflectivity, and mean Doppler velocity measurements, *J. Geophys. Res.*, 108,  
1080 4573, doi:10.1029/2003JD003469, 2003.
- 1081 Donovan, D. P., and van Lammeren, A. C. A. P.: Cloud effective particle size and water  
1082 content profile retrievals using combined lidar and radar observations: 1. Theory and  
1083 examples, *J. Geophys. Res.*, 106, 27,425–27,448, 2001.
- 1084 Donovan, D. P., van Lammeren, A.C.A.P., Hogan, R. J., Russchenberg, H. W. J., Apituley,  
1085 A., Francis, P., Testud, J., Pelon, J., Quante, M., and Goddard, J. W. F.: Cloud effective  
1086 particle size and water content profile retrievals using combined lidar and radar  
1087 observations – 2. Comparison with IR radiometer and in situ measurements of ice  
1088 clouds, *J. Geophys. Res.*, 106, 27449–27464, 2001.
- 1089 Dudhia, J.: Numerical study of convection observed during the winter monsoon  
1090 Experiment using a mesoscale two-dimensional Model, *J. Atmos. Sci.*, 46, 3077–3107,  
1091 <https://doi.org/10.1175/1520-0469>, 1989.
- 1092 Fan, J., Rosenfeld, D., Zhang, Y., Giangrande, S. E., Li, Z., Machado, L. A. T., Martin, S.  
1093 T., Yang, Y., Wang, J., and Artaxo, P.: Substantial convection and precipitation  
1094 enhancements by ultrafine aerosol particles. *Science*, 359, 411–418, 2018
- 1095 Forster, P., et al., Changes in atmospheric constituents and in radiative forcing, in: *Climate*  
1096 *change 2007: the physical science basis*, Contribution of working group I to the Fourth  
1097 Assessment Report of the Intergovernmental Panel on Climate Change, edited by  
1098 Solomon, S., et al., Cambridge Univ. Press, New York, 2007.
- 1099 Gettelman, A., Liu, X., Barahona, D., et al.: Climate impacts of ice nucleation, *J. Geophys.*  
1100 *Res.*, 117, D20201, doi:[10.1029/2012JD017950](https://doi.org/10.1029/2012JD017950), 2012.
- 1101 Gras, J. L.: Southern hemisphere tropospheric aerosol microphysics, *J. Geophys. Res.*, 96,  
1102 5345–5356.
- 1103 Hahn, C. J., and Warren, S. G.: A gridded climatology of clouds over land (1971–96) and  
1104 ocean (1954–97) from surface observations worldwide, *Numeric Data Package NDP-*  
1105 *026EORNL/CDIAC-153*, CDIAC, Department of Energy, Oak Ridge, TN, 2007.

- 1106 Hannak, L., Knippertz, P., Fink, A. H., Kniffka, A., and Pante, G.: Why do global climate  
1107 models struggle to represent low-level clouds in the West African summer monsoon?,  
1108 *J. Climate*, 30, 1665–1687, <https://doi.org/10.1175/JCLI-D-16-0451.1>, 2017
- 1109 Hansen, A., Ament, F., Grutzun, V., and Lammert, A.: Model evaluation by a cloud  
1110 classification based on multi-sensor observations, *Geosci. Model Dev. Discuss.*,  
1111 <https://doi.org/10.5194/gmd-2018-259>, 2018.
- 1112 Hartmann, D. L., Ockert-Bell, M. E., and Michelsen, M. L.: The effect of cloud type on  
1113 earth's energy balance—Global analysis, *J. Climate*, 5, 1281–1304, 1992.
- 1114 Hartmann, M., Gong, X., Kecorius, S., van Pinxteren, M., Vogl, T., Welti, A., Wex, H.,  
1115 Zeppenfeld, S., Herrmann, H., Wiedensohler, A., and Stratmann, F.: Terrestrial or  
1116 marine – indications towards the origin of ice-nucleating particles during melt season  
1117 in the European Arctic up to 83.7° N, *Atmos. Chem. Phys.*, 21, 11613–11636,  
1118 <https://doi.org/10.5194/acp-21-11613-2021>, 2021.
- 1119 Hogan, R. J., Illingworth, A. J., O'Connor, E. J., et al.: Cloudnet: Evaluation of model  
1120 clouds using ground-based observations, *ECMWF Workshop on parametrization of  
1121 clouds on large-scale models.*, 2006.
- 1122 Illingworth, A. J., Hogan, R. J., O'Connor, E. J., et al.: Cloudnet - continuous evaluation of  
1123 cloud profiles in seven operational models using ground-based observations, *Bull. Am.  
1124 Meteorol. Soc.*, 88, 883-898, 2007.
- 1125 IPCC: *Climate Change: The Physical Science Basis. Contribution of Working Group I to  
1126 the Sixth Assessment Report of the Intergovernmental Panel on Climate Change*  
1127 [Masson-Delmotte, V., Zhai, P., Pirani, A., Connors, S. L., Péan, C., Berger, S., Caud,  
1128 N., Chen, Y., Goldfarb, L., Gomis, M. I., Huang, M., Leitzell, K., Lonnoy, E.,  
1129 Matthews, J. B. R., Maycock, T. K., Waterfield, T., Yelekçi, O., Yu, R., and Zhou, B.  
1130 (eds.)]. Cambridge University Press, Cambridge, United Kingdom and New York, NY,  
1131 USA, In press, doi:10.1017/9781009157896, 2021.
- 1132 Jaenicke, R.: Tropospheric aerosols in *Aerosol-Cloud-Climate Interactions*, Hobbs, P. V.,  
1133 ed., Academic Press, San Diego, CA, pp. 1-31.
- 1134 Jiang, H., Feingold, G. and Cotton, W. R: Simulations of aerosol-cloud-dynamical  
1135 feedbacks resulting from entrainment of aerosol into the marine boundary layer during  
1136 the Atlantic Stratocumulus Transition Experiment, *J. Geophys. Res.*, 107(D24), 4813,

- 1137 doi:10.1029/2001JD001502, 2002.
- 1138 Jung, C. H., Yoon, Y. J., Kang, H. J., Gim, Y., Lee, B. Y., Ström, J., Krejci, R., and Tunved,  
1139 P.: The seasonal characteristics of cloud condensation nuclei (CCN) in the arctic lower  
1140 troposphere, *Tellus B: Chemical and Physical Meteorology*, 70:1, 1513291, [https://doi:](https://doi.org/10.1080/16000889.2018.1513291)  
1141 10.1080/16000889.2018.1513291, 2018.
- 1142 Khain, A. P., Ovchinnikov, M., Pinsky, M., Pokrovsky, A. and Krugliak, H.: Notes on the  
1143 state-of-the-art numerical modeling of cloud microphysics, *Atmos. Res.*, 55, 159–224,  
1144 2000.
- 1145 Khain, A., Pokrovsky, A., Rosenfeld, D., Blahak, U., and Ryzhkoy, A.: The role of CCN in  
1146 precipitation and hail in a mid-latitude storm as seen in simulations using a spectral  
1147 (bin) microphysics model in a 2D dynamic frame, *Atmos. Res.*, 99, 129–146, 2011.
- 1148 Khain, A. P., Phillips, V., Benmoshe, N., Pokrovsky, A.: The role of small soluble aerosols  
1149 in the microphysics of deep maritime clouds, *J. Atmos. Sci.*, 69, 2787–2807, 2012.
- 1150 Knippertz, P., Fink, A. H., Schuster, R., Trentmann, J., Schrage, J. M., and Yorke, C.: Ultra-  
1151 low clouds over the southern West African monsoon region, *Geophys. Res. Lett.*, 38,  
1152 L21808, <https://doi.org/10.1029/2011GL049278>, 2011.
- 1153 Korolev, A., and Milbrandt, J.: How are mixed-phase clouds mixed?, *Geophys. Res. Lett.*,  
1154 49, e2022GL099578, 2022.
- 1155 Kogan, Y., 2013: A cumulus cloud microphysics parameterization for cloud-resolving  
1156 models, *J. Atmos. Sci.*, 70, 1423–1436, [https://doi:10.1175/JAS-D-12-0183.1](https://doi.org/10.1175/JAS-D-12-0183.1), 2013.
- 1157 Koop, T., Luo, B. P., Tsias, A., and Peter, T.: Water activity as the determinant for  
1158 homogeneous ice nucleation in aqueous solutions, *Nature*, 406, 611-614.
- 1159 Lee, H., and Baik, J.-J.: A physically based autoconversion parameterization, *J. Atmos. Sci.*,  
1160 74, 1599-1616, <https://doi.org/10.1175/JAS-D-16-0207.1>, 2017.
- 1161 Lee S. S., Penner, J. E., and Saleeby, S. M.: Aerosol effects on liquid-water path of thin  
1162 stratocumulus clouds, *J. Geophys. Res.*, 114, D07204, doi:10.1029/2008JD010513,  
1163 2009.
- 1164 Lee, S. S., et al., Mid-latitude mixed-phase stratocumulus clouds and their interactions with  
1165 aerosols: how ice processes affect microphysical, dynamic and thermodynamic  
1166 development in those clouds and interactions?, *Atmos. Chem. Phys.*,  
1167 <https://doi.org/10.5194/acp-21-16843-2021>, 2021.

- 1168 Li, J., Carlson, B. E., Yung, Y. L., Lv, D., Hansen, J., Penner, J. E., Liao, H., Ramaswamy,  
1169 V., Kahn, R. A., Zhang, P., Dubovik, O., Ding, A., Lacis, A. A., Zhang, L., and Dong,  
1170 Y.: Scattering and absorbing aerosols in the climate system, *Nature Reviews Earth and*  
1171 *Environment*, 3, 363–379, <https://doi.org/10.1038/s43017-022-00296-7>, 2022.
- 1172 Lilly, D. K.: The representation of small scale turbulence in numerical simulation  
1173 experiments, *Proc. Ibm Sci. Comput. Symp. Environ. Sci.*, 320–1951, 195–210, 1967.
- 1174 Lim, K.-S. S., and Hong, S.-Y.: Development of an effective double-moment cloud  
1175 microphysics scheme with prognostic cloud condensation nuclei (CCN) for weather  
1176 and climate models, *Mon. Wea. Rev.*, 138, 1587–1612,  
1177 doi:10.1175/2009MWR2968.1., 2010.
- 1178 Liu, Y., and Daum, P. H.: Parameterization of the autoconversion. Part I: Analytical  
1179 formulation of the Kessler-type parameterizations, *J. Atmos. Sci.*, 61, 1539–1548,  
1180 doi:10.1175/1520-0469(2004)061,1539:POTAPI.2.0.CO;2, 2004.
- 1181 Lohmann, U., and Diehl, K.: Sensitivity studies of the importance of dust ice nuclei for  
1182 the indirect aerosol effect on stratiform mixed-phase clouds, *J. Atmos. Sci.*, 63, 968-  
1183 982, 2006.
- 1184 Mansell, E. R., Ziegler, C. L., and Bruning, E. C., Simulated electrification of a small  
1185 thunderstorm with two-moment bulk microphysics, *J. Atmos. Sci.*, 67, 171–194,  
1186 doi:10.1175/2009JAS2965.1., 2010.
- 1187 Ming, Y., and Chua, X. R.: Convective invigoration traced to warm-rain microphysics,  
1188 *Geophys. Res. Lett.*, 47, doi.org/10.1029/2020GL089134, 2020.
- 1189 Mlawer, E. J., Taubman, S. J., Brown, P. D., Iacono, M. J., and Clough, S. A.: RRTM, a  
1190 validated correlated-k model for the longwave, *J. Geophys. Res.*, 102, 16663-16668,  
1191 1997.
- 1192 Moeng, C.-H., Sullivan, P. P., and Stevens, B.: Including radiative effects in an entrainment  
1193 rate formula for buoyancy-driven PBLs, *J. Atmos. Sci.*, 56, 1031 – 1049,  
1194 doi:10.1175/1520-0469(1999)056<1031:IREIAE>2.0.CO;2, 1999.
- 1195 Möhler, O., et al, Efficiency of the deposition mode ice nucleation on mineral dust particles,  
1196 *Atmos. Chem. Phys.*, 6, 3007-3021, 2006.
- 1197 Morrison, H., deBoer, G., Feingold, G., Harrington, J., Shupe, M., and Sulia, K., Resilience  
1198 of persistent Arctic mixed-phase clouds, *Nat. Geosci.*, 5, 11–17,

- 1199 <https://doi.org/10.1038/ngeo1332>, 2012.
- 1200 Morrison, H., Curry, J. A., and Khvorostyanov, V. I., A new double-moment microphysics  
1201 parameterization for application in cloud and climate models. Part I: Description, *J.*  
1202 *Atmos. Sci.*, 62, 1665–1677, 2005.
- 1203 Morrison, H., hompson, G., and V. Tatarskii, Impact of cloud microphysics on the  
1204 development of trailing stratiform precipitation in a simulated squall line: Comparison  
1205 of one- and two-moment schemes. *Mon. Wea. Rev.*, 137, 991–1007,  
1206 <https://doi.org/10.1175/2008MWR2556.1>, 2009.
- 1207 Murakami, M., 1990, Numerical modeling of the dynamical and microphysical evolution  
1208 of an isolated convective cloud—The July 19 1981 CCOPE cloud, *J. Meteor. Soc.*  
1209 *Japan*, 68, 107–128.
- 1210 Ovchinnikov, M., Korolev, A., and Fan, J.: Effects of ice number concentration on  
1211 dynamics of a shallow mixed-phase stratiform cloud, *J. Geophys. Res.*, 116, D00T06,  
1212 doi:10.1029/2011JD015888, 2011.
- 1213 Possner, A., Ekman, A. M. L., and Lohmann, U.: Cloud response and feedback processes  
1214 in stratiform mixed-phase clouds perturbed by ship exhaust, *Geophys. Res. Lett.*, 44,  
1215 1964–1972, <https://doi.org/10.1002/2016GL071358>, 2017.
- 1216 Pruppacher, H. R. and Klett, J. D.: *Microphysics of clouds and precipitation*, 714pp, D.  
1217 Reidel, 1978.
- 1218 Ramaswamy, V., et al.: Radiative forcing of climate change, in *Climate Change 2001: The*  
1219 *Scientific Basis*, edited by J. T. Houghton et al., 349-416, Cambridge Univ. Press,  
1220 New York, 2001.
- 1221 Schima, J., McFarquhar, G., Romatschke, U., Vivekanandan, J., D’Alessandro, J., Haggerty,  
1222 et al.: Characterization of Southern Ocean boundary layer clouds using airborne radar,  
1223 lidar, and in situ cloud data: Results from SOCRATES, *J. Geophys. Res.*, 127,  
1224 e2022JD037277, 2022.
- 1225 Seinfeld, J. H., and Pandis, S. N.: *Atmospheric chemistry and physics: From air pollution*  
1226 *to climate change*, John Wiley & Sons, 1326 pp, 1998.
- 1227 Solomon, A., de Boer, G., Creamean, J. M., McComiskey, A., Shupe, M. D., Maahn, M.,  
1228 and Cox, C.: The relative impact of cloud condensation nuclei and ice nucleating  
1229 particle concentrations on phase partitioning in Arctic mixed-phase stratocumulus



- 1230 clouds, *Atmos. Chem. Phys.*, 18, 17047–17059, [https://doi.org/10.5194/acp-18-](https://doi.org/10.5194/acp-18-17047-2018)  
1231 17047-2018, 2018.
- 1232 Smagorinsky, J.: General circulation experiments with the primitive equations, *Mon. Wea.*  
1233 *Rev.*, 91, 99–164, 1963.
- 1234 Stevens, B., et al.: On entrainment rates in nocturnal marine stratocumulus, *Q. J. R.*  
1235 *Meteorol. Soc.*, 129, 3469 – 3492, doi:10.1256/qj.02.202, 2003a.
- 1236 Stevens, B., et al.: Dynamics and chemistry of marine stratocumulus-DYCOMS-II, *Bull.*  
1237 *Am. Meteorol. Soc.*, 84, 579– 593, doi:10.1175/BAMS-84-5-579, 2003b.
- 1238 Stevens, B., and Feingold, G.: Untangling aerosol effects on clouds and precipitation in a  
1239 buffered system, *Nature*, 461, 607–613, <https://doi.org/10.1038/nature08281>, 2009.
- 1240 Stephens, G. L., and Greenwald, T. J.: Observations of the Earth’s radiation budget in  
1241 relation to atmospheric hydrology. Part II: Cloud effects and cloud feedback, *J.*  
1242 *Geophys. Res.*, 96, 15 325–15 340, 1991.
- 1243 Tinel, C., Testud, J., Hogan, R. J., Protat, A., Delanoe, J. and Bouniol, D.: The retrieval of  
1244 ice cloud properties from cloud radar and lidar synergy, *J. Appl. Meteorol.*, 44, 860-  
1245 875, 2005.
- 1246 Tsushima, Y., Webb, M. J., Williams, K. D., Soden, B. J., et al.: Importance of the mixed-  
1247 phase cloud distribution in the control climate for assessing the response of clouds to  
1248 carbon dioxide increase: A multi-model study, *Clim. Dyn.*, 27, 113–126, 2006.
- 1249 Tunved, P., Ström, J. and Krejci, R.: Arctic aerosol life cycle: linking aerosol size  
1250 distributions observed between 2000 and 2010 with air mass transport and  
1251 precipitation at Zeppelin station, Ny-Ålesund, Svalbard, *Atmos. Chem. Phys.*,  
1252 13, 3643–3660, <https://doi.org/10.5194/acp-13-3643-2013>, 2013
- 1253 Twomey, S.: Pollution and the Planetary Albedo, *Atmos. Env.*, 8,1251-1256, 1974.
- 1254 Warren, S. G., Hahn, C. J., London, J., Chervin, R. M., and Jenne, R. L.: Global distribution  
1255 of total cloud cover and cloud types over land, NCAR Tech. Note NCAR/TN-  
1256 273+STR, National Center for Atmospheric Research, Boulder, CO, 29 pp. + 200  
1257 maps, 1986.
- 1258 Wood, R.: Stratocumulus clouds, *Mon. Wea. Rev.*, 140, 2373-2423, 2012.
- 1259 Xue, L., Teller, A., Rasmussen, R. M., Geresdi, I., and Pan, Z.: Effects of aerosol solubility  
1260 and regeneration on warm-phase orographic clouds and precipitation simulated by a

1261 detailed bin microphysical scheme, *J. Atmos. Sci.*, 67, 3336–3354, 2010.

1262 Zhang, D., Vogelmann, A., Kollias, P., Luke, E., Yang, F., Lubin, D., and Wang, Z.:  
1263 Comparison of Antarctic and Arctic single-layer stratiform mixed-phase cloud  
1264 properties using ground-based remote sensing measurements, *J. Geophys. Res.*, 124,  
1265 10186–10204, <https://doi.org/10.1029/2019JD030673>, 2019.

1266 Zheng, Y., Zhang, H., Rosenfeld, D., Lee, S. S., Su, T., and Li, Z.: Idealized Large-Eddy  
1267 Simulations of Stratocumulus Advecting over Cold Water. Part I: Boundary Layer  
1268 Decoupling, 78, 4089-4102, <https://doi.org/10.1175/JAS-D-21-0108.1>, 2021.

1269

1270

1271

1272

1273

1274

1275

1276

1277

1278

1279

1280

1281

1282

1283

1284

1285

1286

1287

1288

1289

1290

1291

1292

1293

1294

1295

1296

1297

1298

1299

1300

1301

1302

1303 **FIGURE CAPTIONS**

1304

1305 Figure 1. A red rectangle marks the simulation domain in the Svalbard area, Norway, and  
1306 a dot in the rectangle marks a ground station which is a part of the Cloudnet observation  
1307 network. The light blue represents the ocean and the green the land area.

1308

1309 Figure 2. (a) The vertical distributions of the domain-averaged potential temperature and  
1310 humidity at the first time step, (b) the time series of the domain-averaged large-scale  
1311 subsidence or downdraft at the model top and (c) the time series of the domain-averaged  
1312 surface temperature.

1313

1314 Figure 3. Aerosol size distribution at the surface.  $N$  represents aerosol number  
1315 concentration per unit volume of air and  $D$  represents aerosol diameter.

1316

1317 Figure 4. The vertical distributions of the time- and domain-averaged IWC and LWC in  
1318 the 200\_2 and 200\_0 runs.

1319

1320 Figure 5. The time series of (a) observed and simulated cloud-top and bottom heights, (b)  
1321 retrieved and simulated IWP, and observed and simulated LWP, and (c) the simulated  
1322 surface sensible and latent heat fluxes. Observed and retrieved values are from the ground  
1323 station as marked in Figure 1. For the time series, in the simulation domain, the simulated  
1324 cloud-top height is averaged over grid points with cloud tops and the simulated cloud-  
1325 bottom height is averaged over grid points with cloud bottoms, while the simulated IWP  
1326 and LWP are averaged over grid points with non-zero IWP and LWP, respectively, at each  
1327 time step in the 200\_2 run. The simulated surface sensible and latent heat fluxes are  
1328 averaged over the horizontal domain at the surface and each time step in the 200\_2 run.

1329

1330 Figure 6. The vertical distributions of the time- and domain-averaged deposition and  
1331 condensation rates in the 200\_2 and 200\_0 runs.

1332

1333 Figure 7. The time series of the average supersaturation with respect to ice and water over  
1334 grid points where deposition occurs in the presence of both droplets and ice crystals in the  
1335 200\_2 run.

1336 Figure 8. The vertical distributions of the time- and domain-averaged IWC and LWC in  
1337 the 200\_2, 200\_0 and 200\_0.07 runs.

1338

1339 Figure 9. The vertical distributions of the time- and domain-averaged (a) IWC in the 200\_2,  
1340 2000\_20, 200\_0.07, 200\_20, 2000\_2, 2000\_0.07, and 200\_0.7 runs. (b) The vertical  
1341 distributions of the time- and domain-averaged LWC in the 200\_0 and 2000\_0 runs as well  
1342 as all the runs shown in panel (a).

1343

1344 Figure 10. The average size distributions of (a) ice crystals over grid points with non-zero  
1345 IWC and the simulation period and (b) drops over grid points with non-zero LWC and the  
1346 simulation period.

1347

1348 Figure 11. IWC/LWC as a function of ICNCavg/CDNCavg based on Table 4.

1349

1350

1351

1352

1353

1354

1355

1356

1357

1358

1359

1360

1361

1362

1363

Simulations	The number concentration of aerosols acting as CCN at the first time step in the PBL (cm <sup>-3</sup> )	The number concentration of aerosols acting as INP at the first time step in the PBL (cm <sup>-3</sup> )	ICNCavg/CDNCavg	Ice processes	Radiation
200 2	200	2	0.220	Present	Present
2000 20	2000	20	0.201	Present	Present
2000 2	2000	2	0.108	Present	Present
200 20	200	20	0.512	Present	Present
200 0	200	2	0.000	Absent	Present
2000 0	2000	2	0.000	Absent	Present
200 0.07	200	0.07	0.022	Present	Present
2000 0.07	2000	0.07	0.012	Present	Present
200 0.7	200	0.7	0.041	Present	Present
4000 45	4000	45	0.220	Present	Present
13 0.1	13	0.1	0.220	Present	Present
4000 1.8	4000	1.8	0.022	Present	Present
12 0.0035	12	0.0035	0.022	Present	Present

1364

1365 Table 1. Summary of simulations

1366

1367

1368

1369

1370

1371

1372

1373

1374

1375

1376

1377

1378

1379

1380

1381

Simulations	IWC ( $10^{-3}$ $\text{g m}^{-3}$ )	LWC ( $10^{-3}$ $\text{g m}^{-3}$ )	IWP ( $\text{g m}^{-2}$ )	LWP ( $\text{g m}^{-2}$ )	IWC/LWC	IWP/LWP	Condensation rate		Deposition rate		Cloud-base sedimentation ( $10^{-3} \text{g m}^{-2} \text{s}^{-1}$ )		Entrainment ( $\text{cm s}^{-1}$ )
							Over grid points ( $10^{-2}$ $\text{g m}^{-3}$ $\text{s}^{-1}$ )	Over cloudy columns ( $\text{g m}^{-2}$ $\text{s}^{-1}$ )	Over grid points ( $10^{-2}$ $\text{g m}^{-3}$ $\text{s}^{-1}$ )	Over cloudy columns ( $\text{g m}^{-2}$ $\text{s}^{-1}$ )	Ice- crystal	Droplet	
200 2	6.57	0.25	31.94	1.23	26.28	25.96	0.11	1.98	1.30	23.40	1.17	0.17	0.25
2000 20	7.82	0.21	40.91	1.08	37.24	37.91	0.09	1.62	1.57	28.26	0.94	0.06	0.53
2000 2	6.55	0.29	31.85	1.46	22.58	21.81	0.12	2.16	1.28	23.04	1.11	0.08	0.28
200 20	7.80	0.20	40.82	1.01	39.00	40.42	0.09	1.62	1.56	28.08	0.97	0.11	0.51
200 0	0.00	2.06	0.00	10.35	0.00	0.00	0.72	12.48	0.00	0.00	0.00	0.36	0.08
2000 0	0.00	2.25	0.00	11.29	0.00	0.00	0.76	12.80	0.00	0.00	0.00	0.14	0.10
200 0.07	0.89	0.85	4.27	4.20	1.05	1.02	0.32	5.76	0.35	6.30	0.19	0.28	0.06
2000 0.07	0.79	0.97	3.82	4.83	0.81	0.79	0.38	6.84	0.31	5.58	0.17	0.19	0.07
200 0.7	0.98	0.78	4.73	3.88	1.25	1.22	0.31	5.58	0.39	7.02	0.14	0.22	0.07

1382

1383 Table 2. The averaged IWC, LWC, IWP, LWP, condensation and deposition rates over all  
1384 of grid points and the simulation period in each of simulations. IWC/LWC (IWP/LWP) is  
1385 the averaged IWC (IWP) over the averaged LWC (LWP). Also, as shown are the vertically  
1386 integrated condensation and deposition rates over each cloudy column which are averaged  
1387 over those columns and the simulation period. The average cloud-base sedimentation rate,  
1388 which is for each of ice crystals and droplets, over the cloud base and simulation period,  
1389 and the average cloud-top entrainment rate over the cloud top and simulation period are  
1390 shown as well.

1391

1392

1393

1394

1395

1396

1397

1398

1399

1400

1401

1402

1403

1404

Simulations	IWC ( $10^{-3}$ $\text{g m}^{-3}$ )	LWC ( $10^{-3}$ $\text{g m}^{-3}$ )	IWP ( $\text{g m}^{-2}$ )	LWP ( $\text{g m}^{-2}$ )	IWC/LWC	IWP/LWP	Condensation rate		Deposition rate		Cloud-base sedimentation ( $10^{-3} \text{g m}^{-2} \text{s}^{-1}$ )		Entrainment ( $\text{cm s}^{-1}$ )
							Over grid points ( $10^{-2}$ $\text{g m}^{-3}$ $\text{s}^{-1}$ )	Over cloudy columns ( $\text{g m}^{-2}$ $\text{s}^{-1}$ )	Over grid points ( $10^{-2}$ $\text{g m}^{-3}$ $\text{s}^{-1}$ )	Over cloudy columns ( $\text{g m}^{-2}$ $\text{s}^{-1}$ )	Ice- crystal	Droplet	
200 2 norad	6.42	0.24	31.21	1.22	26.75	25.58	0.10	1.96	1.29	23.35	1.16	0.16	0.24
2000 20 norad	7.63	0.21	40.05	1.07	36.33	37.42	0.09	1.59	1.55	29.91	0.92	0.06	0.51
2000 2 norad	6.40	0.29	31.11	1.45	22.06	21.45	0.11	2.12	1.26	22.69	1.07	0.08	0.27
200 20 norad	7.61	0.20	39.95	0.99	38.05	40.35	0.09	1.59	1.54	27.72	0.97	0.11	0.49
200 0 norad	0.00	2.03	0.00	10.20	0.00	0.00	0.72	12.31	0.00	0.00	0.00	0.34	0.08
2000 0 norad	0.00	2.21	0.00	11.12	0.00	0.00	0.75	12.63	0.00	0.00	0.00	0.13	0.10
200 0.07 norad	0.87	0.84	4.21	4.17	1.04	1.01	0.31	5.74	0.35	6.21	0.18	0.27	0.05
2000 0.07 norad	0.78	0.96	3.78	4.80	0.81	0.79	0.36	6.81	0.30	5.50	0.16	0.18	0.06
200 0.7 norad	0.97	0.76	4.70	3.85	1.25	1.22	0.30	5.55	0.38	6.91	0.13	0.21	0.06

1405

1406 Table 3. Same as Table 2 but for the repeated simulations with radiative processes turned

1407 off.

1408

1409

1410

1411

1412

1413

1414

1415

1416

1417

1418

1419

1420

1421

1422

1423

1424

1425

1426

1427

Simulations	ICNCavg/CDNCavg	Percentage increases (+) or decrease (-) in ICNCavg/CDNCavg	IWC/LWC	Percentage increases (+) or decrease (-) in IWC/LWC
2000 0.07	0.012		0.81	
200 0.07	0.022	+83.33%	1.05	+29.6%
200 0.7	0.041	+86.36%	1.25	+19.0%
2000 2	0.108	+163.4%	22.58	+1706.4%
2000 20	0.201	+86.1%	37.24	+64.9%
200 2	0.220	+9.4%	26.28	-29.4%
200 20	0.512	+132.7%	39.00	+48.4%

1428

1429 Table 4. ICNCavg/CDNCavg and IWC/LWC in the simulations that are related to Section

1430 4.1. The Percentage increases or decreases in ICNCavg/CDNCavg and IWC/LWC as

1431 shown in the  $i^{\text{th}}$  row are  $\frac{(\text{ICNCavg/CDNCavg})_i - (\text{ICNCavg/CDNCavg})_{i-1}}{(\text{ICNCavg/CDNCavg})_{i-1}} \times 100 (\%)$  and1432  $\frac{(\text{IWC/LWC})_i - (\text{IWC/LWC})_{i-1}}{(\text{IWC/LWC})_{i-1}} \times 100 (\%)$ , respectively. Here,  $(\text{ICNCavg/CDNCavg})_i$  and1433  $(\text{IWC/LWC})_i$  represent ICNCavg/CDNCavg and IWC/LWC in the  $i^{\text{th}}$  row, respectively.

1434

1435

1436

1437

1438

1439

1440

1441

1442

1443

1444

1445

1446

1447

1448

1449

1450



Simulations	ICNCavg/CDNCavg	IWC/LWC	Percentage increases (+) or decrease (-) in IWC/LWC
Polar case			
200_2	0.220	26.28	
4000_45	0.220	27.25	+3.7%
13_0.1	0.220	25.62	-2.5%
Representing midlatitude case			
200_0.07	0.022	1.05	
4000_1.8	0.022	1.09	+3.8%
12_0.0035	0.022	1.02	-2.9%

1451

1452 Table 5. ICNCavg/CDNCavg and IWC/LWC in the simulations that are related to Section  
1453 4.2. The percentage increases or decreases in IWC/LWC in the 4000\_45 run or in the

1454 13\_0.1 run are  $\frac{(IWC/LWC)_{4000\_45 \text{ or } 13\_0.1} - (IWC/LWC)_{200\_2}}{(IWC/LWC)_{200\_2}} \times 100 (\%)$ . Here,

1455  $(IWC/LWC)_{4000\_45 \text{ or } 13\_0.1}$  represents IWC/LWC in the 4000\_45 run or the 13\_01 run, while

1456  $(IWC/LWC)_{200\_2}$  represents IWC/LWC in the 200\_2 run. The percentage increases or

1457 decreases in IWC/LWC in the 4000\_1.8 run or the 12\_0.0035 run are

1458  $\frac{(IWC/LWC)_{4000\_1.8\_fac10 \text{ or } 12\_0.0035\_fac10} - (IWC/LWC)_{200\_2\_fac10}}{(IWC/LWC)_{200\_2\_fac10}} \times 100 (\%)$ . Here,

1459  $(IWC/LWC)_{4000\_1.8 \text{ or } 12\_0.0035}$  represents IWC/LWC in the 4000\_1.8 run or the 12\_0.0035

1460 run, while  $(IWC/LWC)_{200\_0.07}$  represents IWC/LWC in the 200\_0.07 run.

1461

1462

1463

1464

1465

1466

1467

1468

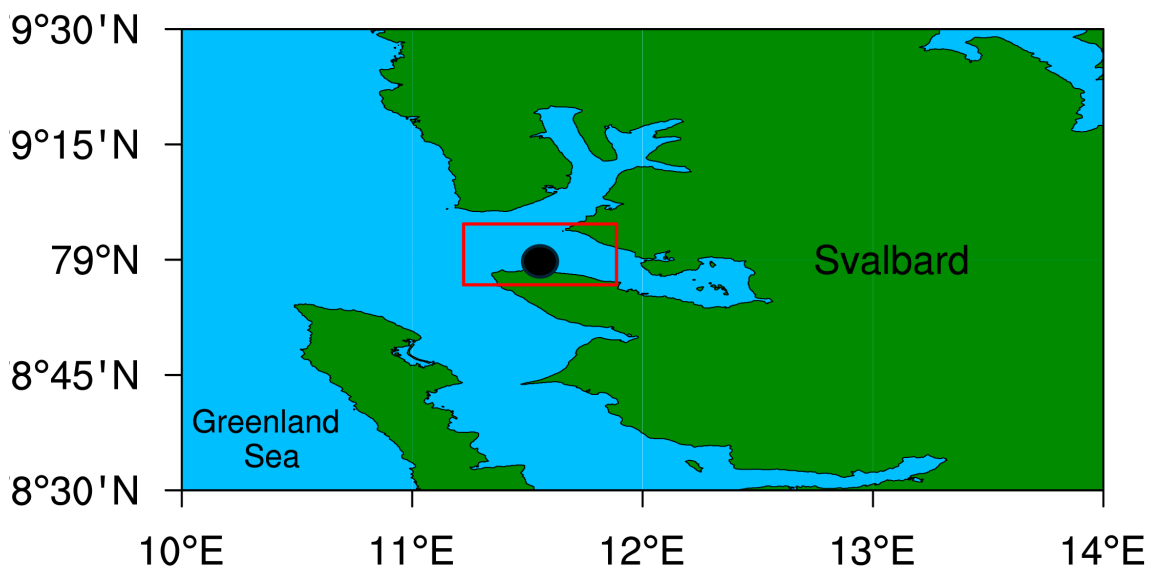
1469

1470

1471

1472

1473



1474

1475

**Figure 1**

1476

1477

1478

1479

1480

1481

1482

1483

1484

1485

1486

1487

1488

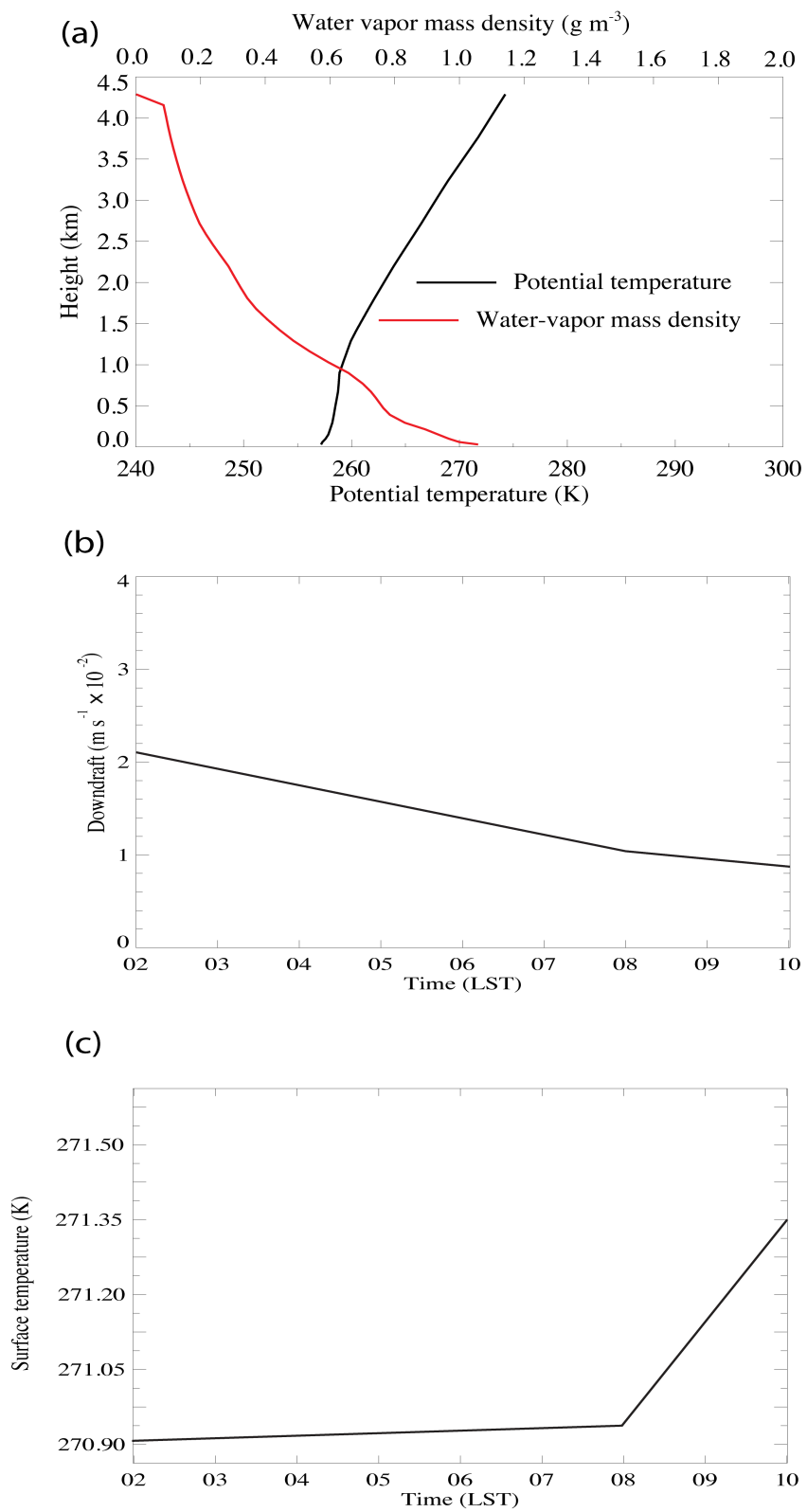
1489

1490

1491

1492

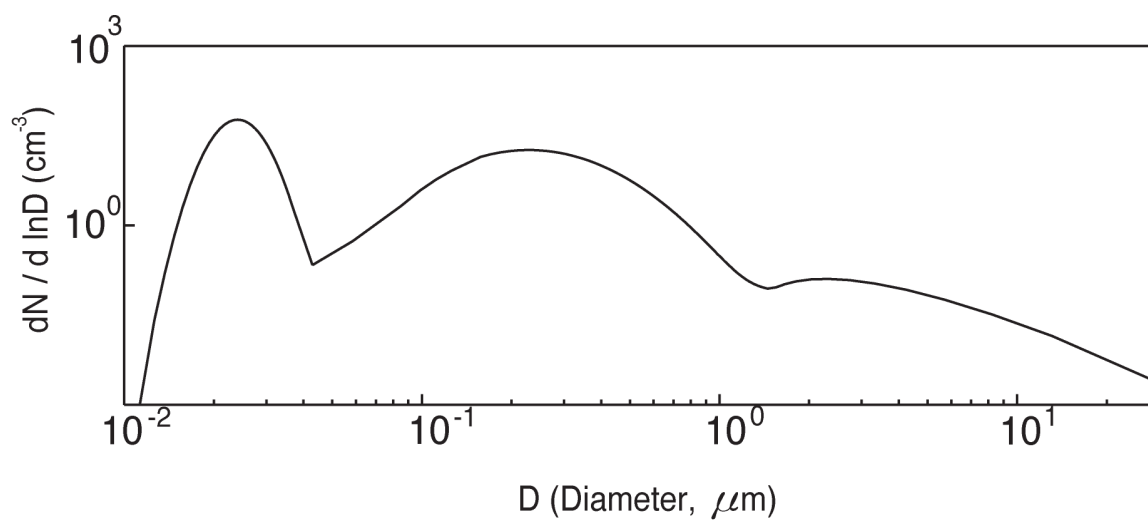
1493



1494

1495

Figure 2



1496

1497

**Figure 3**

1498

1499

1500

1501

1502

1503

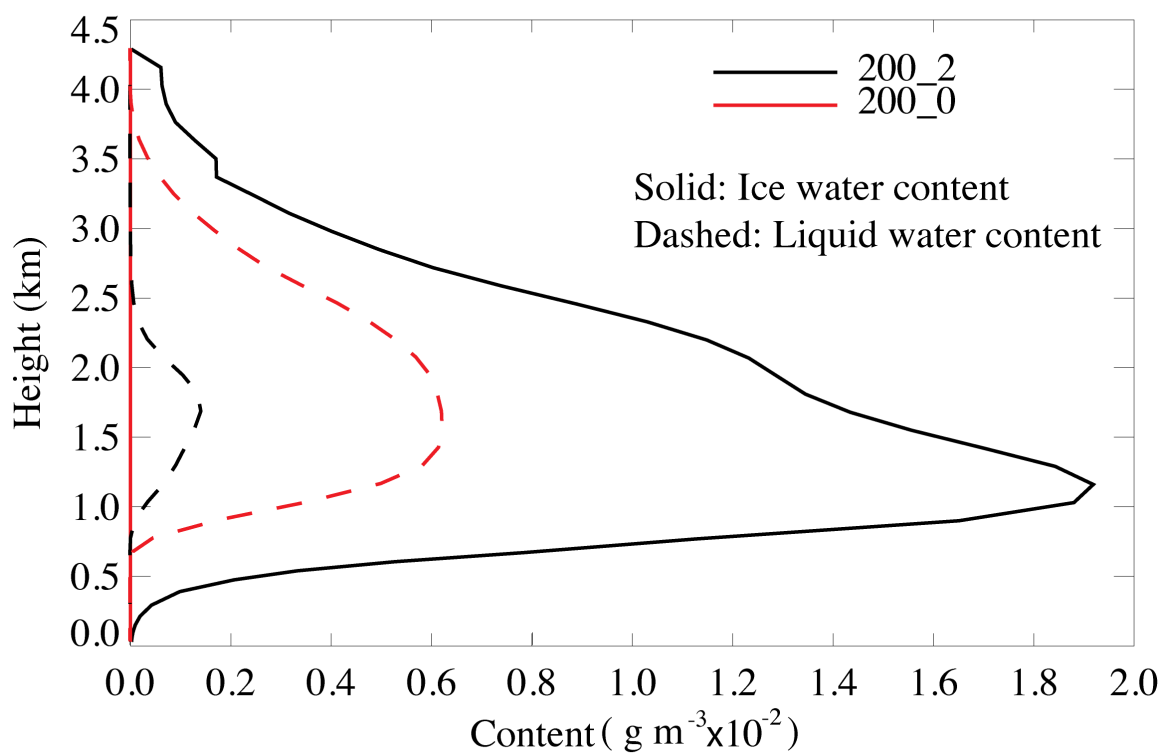
1504

1505

1506

1507

1508



1509

1510

**Figure 4**

1511

1512

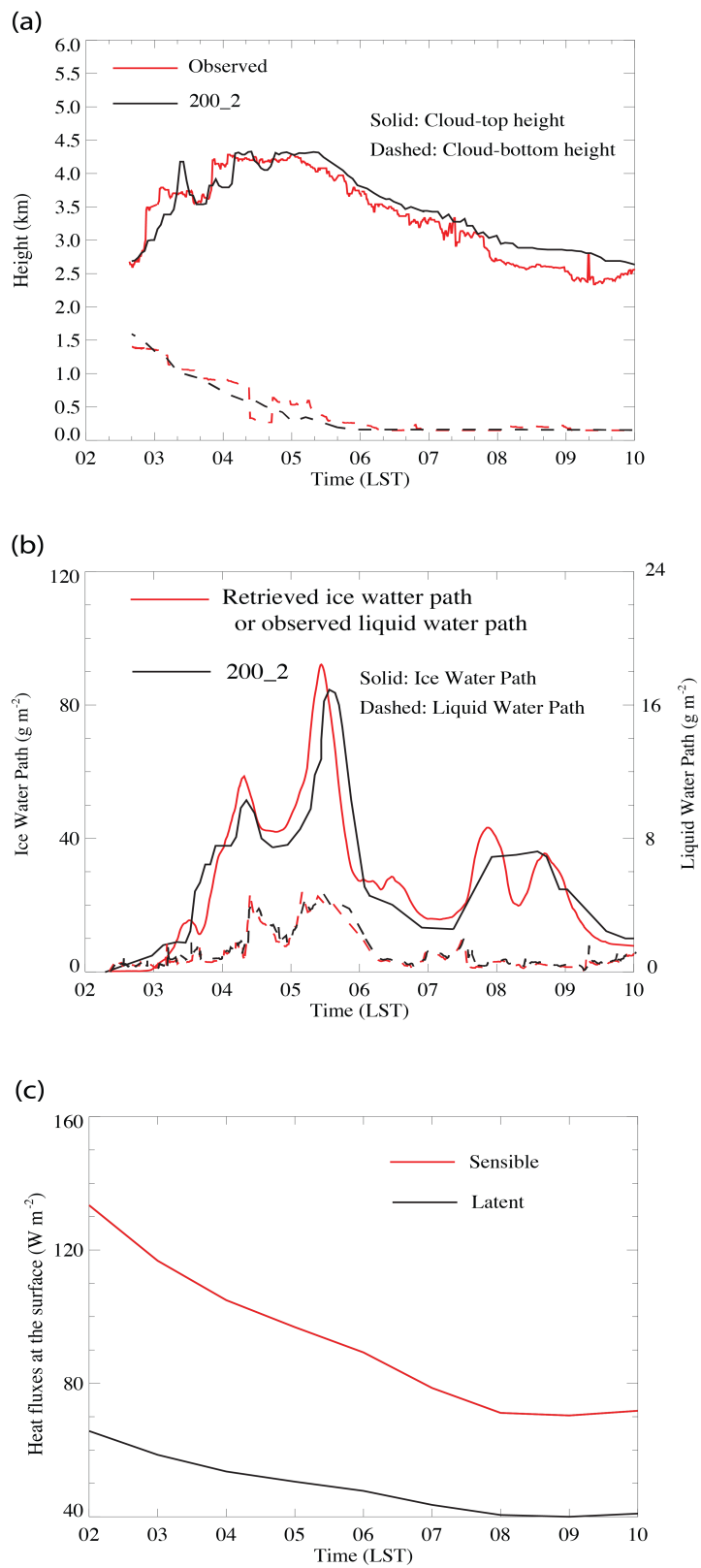
1513

1514

1515

1516

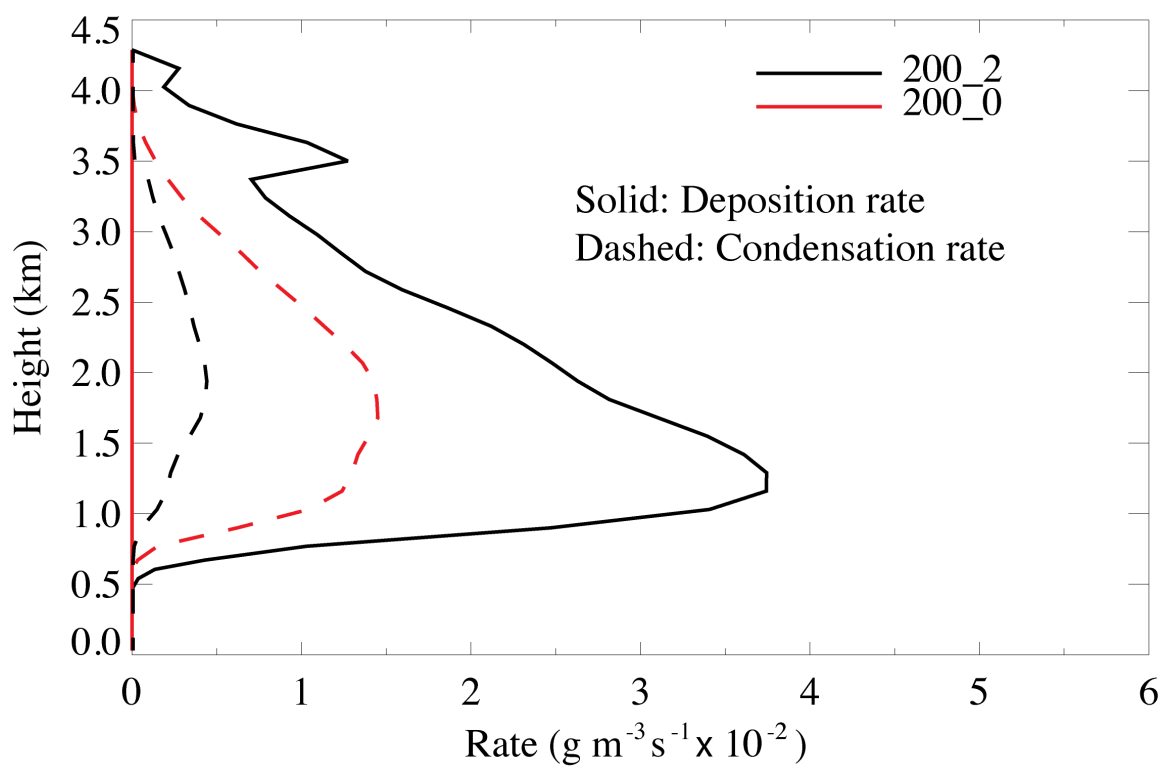
1517



1518

1519

Figure 5



1520

1521

**Figure 6**

1522

1523

1524

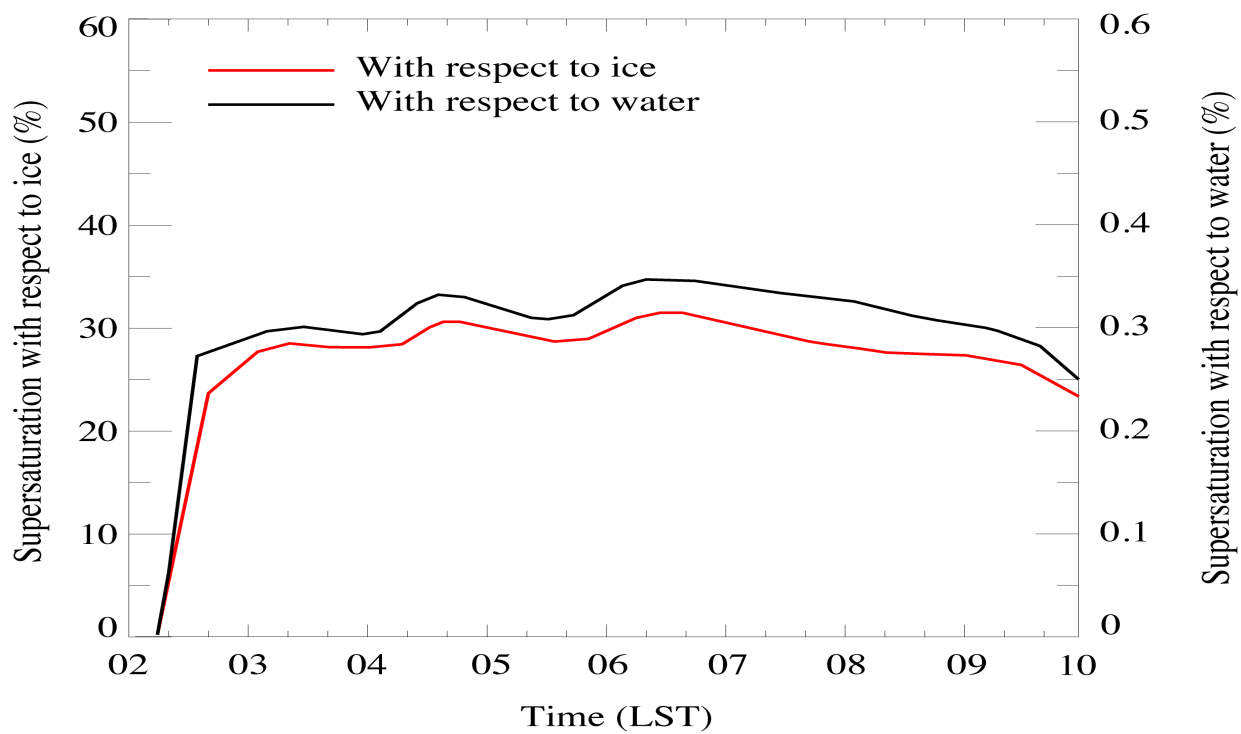
1525

1526

1527

1528

1529



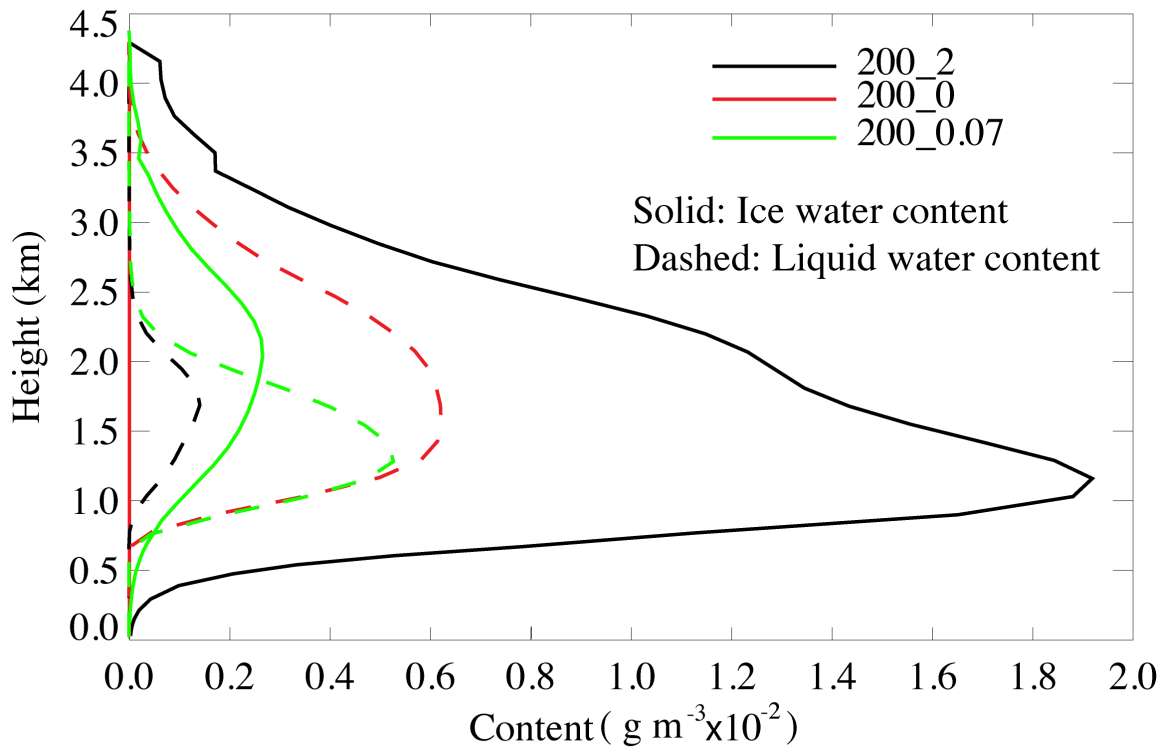
1530

1531

1532

**Figure 7**





1533

1534

**Figure 8**

1535

1536

1537

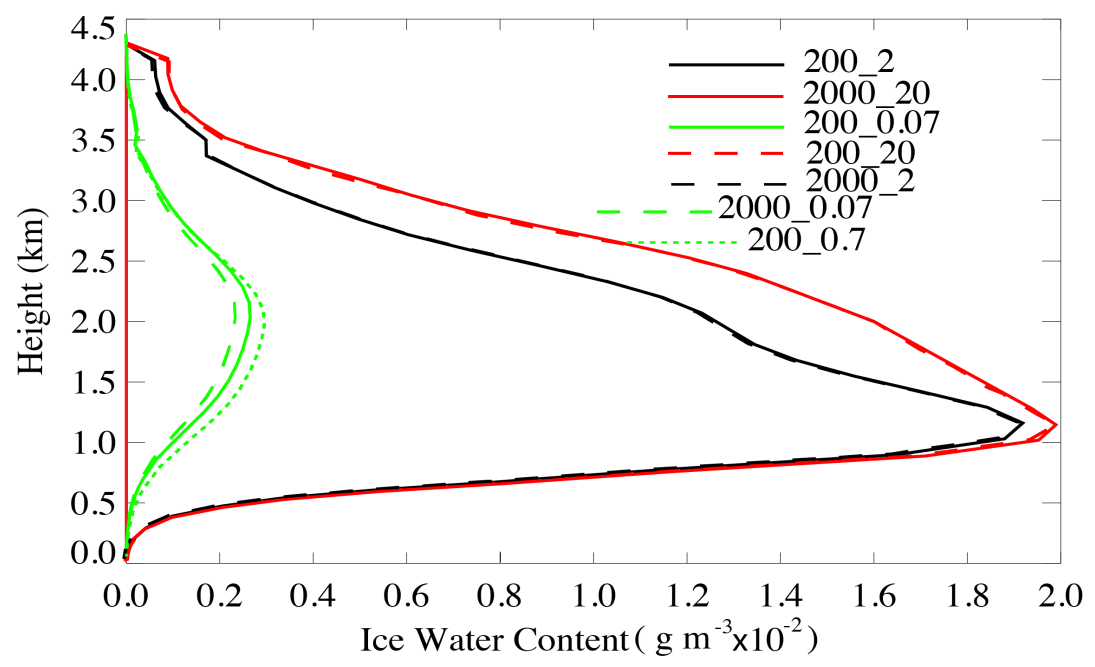
1538

1539

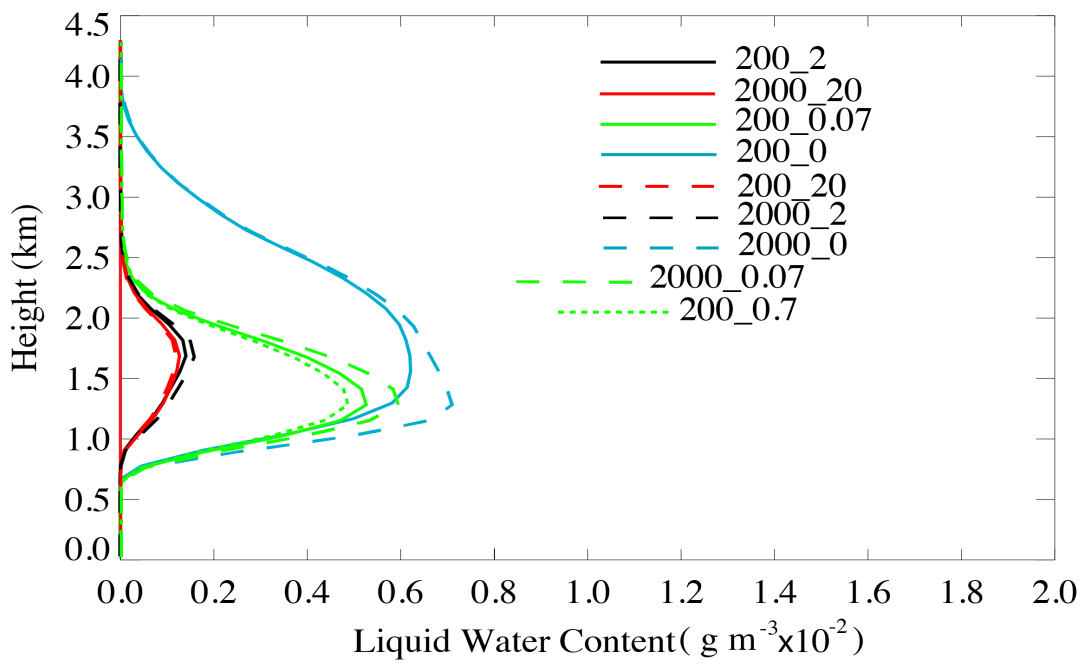
1540

1541

(a)



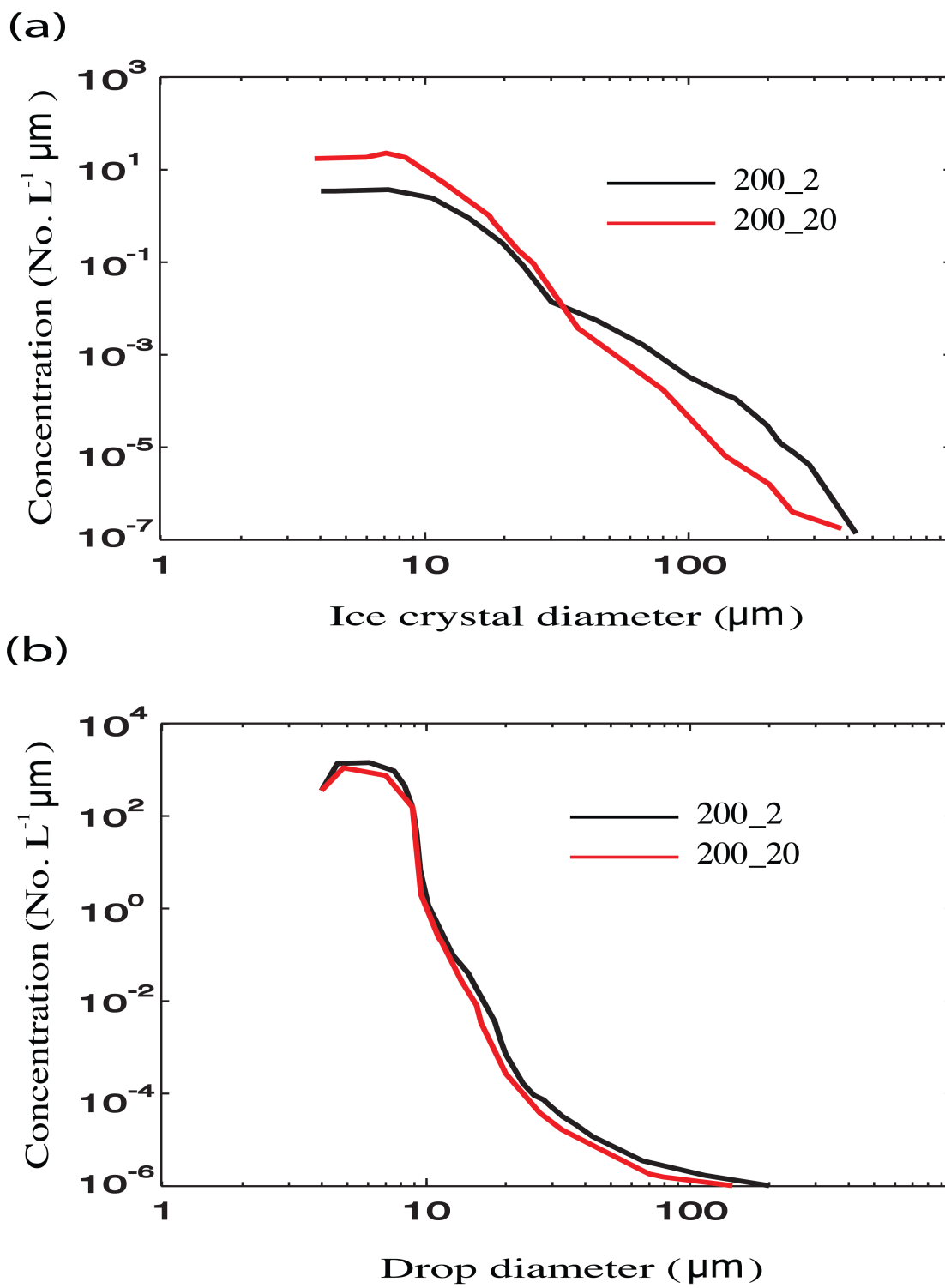
(b)



1542

1543

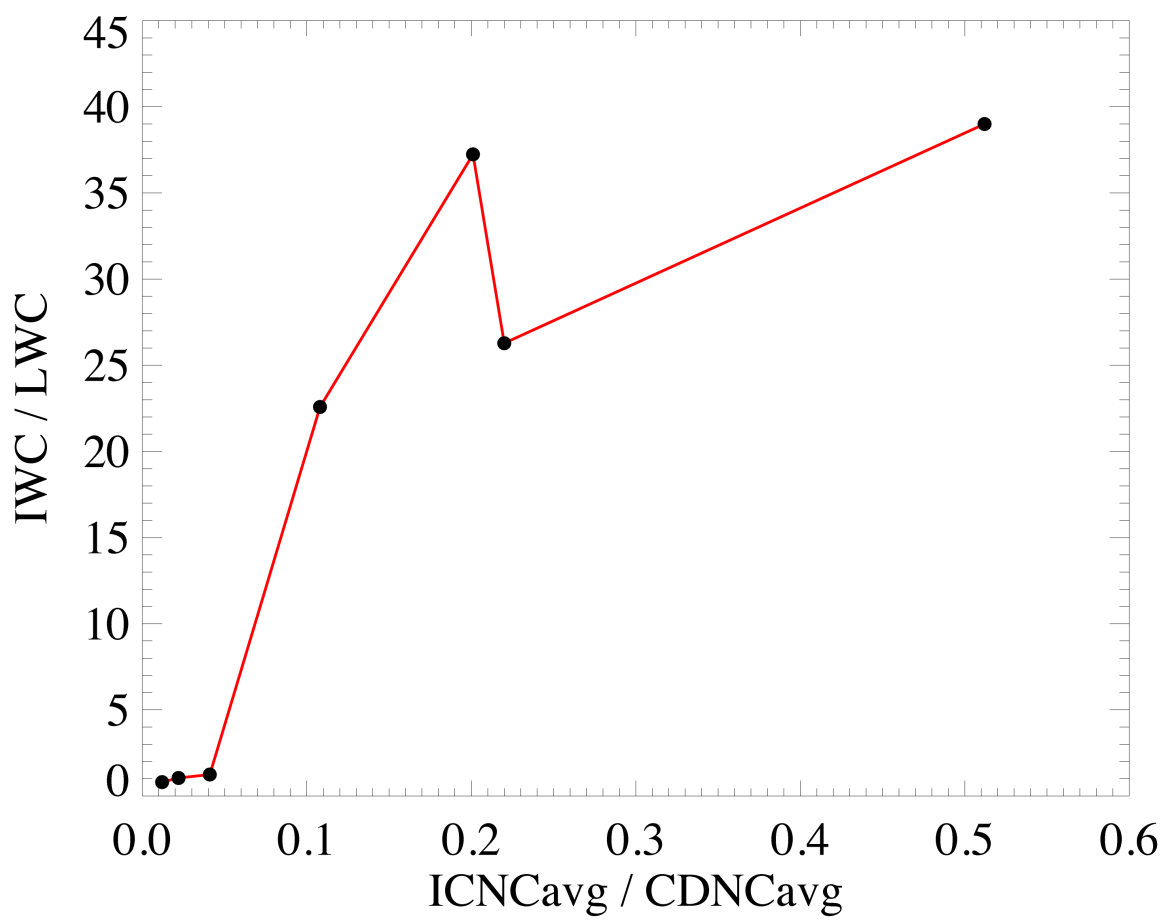
Figure 9



1544

1545

**Figure 10**



1546

1547

1548

**Figure 11**